The Swiss - Norwegian Beam Lines at ESRF

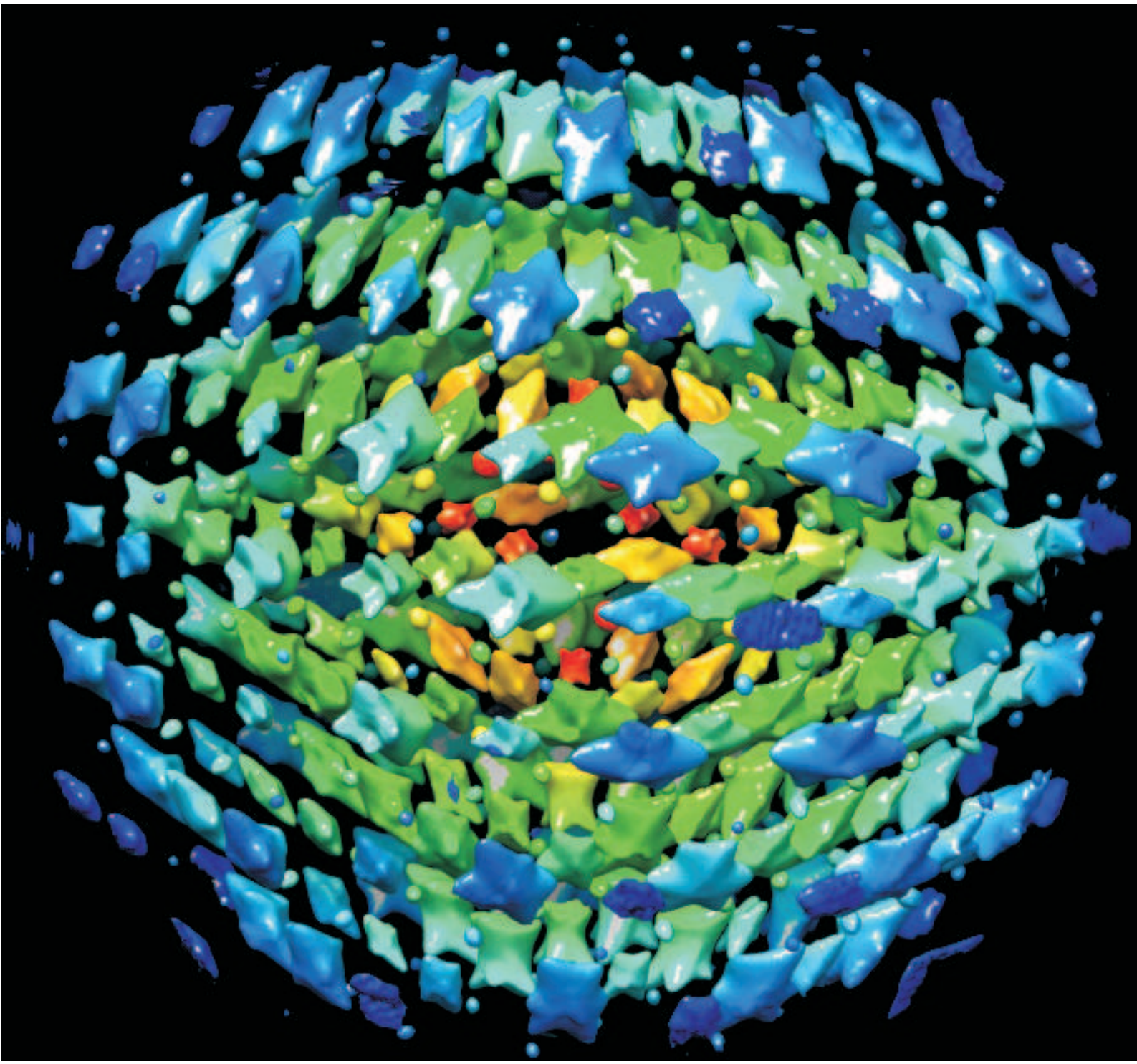

11/12

ACTIVITY REPORT

CONTENTS

INTRODUCTION

The years 2009-2012 have finalized a very important period in the life of SNBL. Following the report of the SNBL Committee of the Future in 2008, several areas for new investment were identified. Where sufficient resources were available, the recommendations have been rapidly implemented during this period. The extensive capability for performing in-situ experiments now available at SNBL is a good example of this kind of investment. Where external support was required, the user community (in concert with the in-house staff) has been very successful in raising the necessary funds. Therefore, both of the beamlines have seen major upgrades over the last few years. These have been aimed both at bringing the beamline infrastructure and controls up to the latest standards, and at installing and commissioning new instrumentation. The largest single investment has been the Pilatus2M detector and associated diffractometry. The required additional funding (in excess of €1M) was provided jointly by the research councils of Switzerland and Norway.

In 2012, Swiss and Norwegian administrations considered the renewal of the four-year bi-national agreement for SNBL, and asked for a new budget to be defined which was commensurate with its goals. In this context, a number of questions were addressed. Is the technical status of the beamline and its instrumentation well correlated to the research interests of synchrotron users in general and, more especially, how does it relate to the scientific activities of the Swiss and Norwegian academic communities? What instrumentation is needed in order to keep the facility attractive and competitive, bearing in mind that many new beamlines are under construction both within the ESRF and elsewhere in Europe?

Before signing the Agreement and Memorandum, discussions organised in both countries showed a continued and wide interest within the Swiss and Norwegian synchrotron communities to run the SNBL's beyond the actual budget period. Moreover, the SNX-Council received a strong commitment from the Norwegian and Swiss administrations for their continuous support. It is therefore a pleasure to be able to report that the SNBL SNX Cooperation Agreement and Memorandum of Understanding for the period 2013-2016, together with a generous funding profile from both Norway (RCN) and Switzerland (SERI), has been approved by both countries. Thus, we can safely claim today that the long-term perspectives of the Swiss-Norwegian CRG are secured until 2017 and look very promising beyond, and we look forward to maintaining and developing the service which we provide to our user community.

V. DMITRIEV, P. PATTISON, H. EMERICH

SCIENTIFIC HIGHLIGHTS

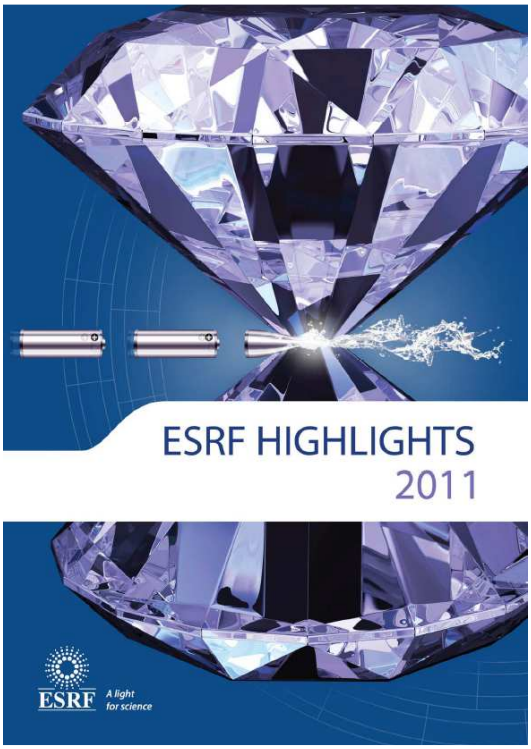

Molecular near-infrared to visible light upconversion

Near-Infrared to visible photon up-conversion is a process in which photoexcitation at a certain wavelength in the near infrared is followed by luminescence at a shorter wavelength in the visible. In this process, low energy photons are "converted" to higher energy photons. This phenomenon could be of potential use in liquid solar cell applications in order take advantage of the infrared part of the solar spectrum or in biological imaging to design visible emitting bio-luminescent probes which are excited with infrared radiation. Using a longer excitation wavelength than in the visible range, infrared presents several advantages such as less phototoxicity and a deeper penetration depth into living tissues. Moreover, compared to classical fluorescence spectroscopy, up-conversion microscopy does not suffer from noise due to the auto-luminescence of the sample [1].

where the geometry of the metal centre is controlled. This control enables chemists to synthesise assemblies with specific structural properties in order to tune the physical properties.

With a two-photon excitation model in mind, we therefore designed a molecular complex which can maximise the probability of the ETU process. It consists of the connection of two chromium(III) sensitisers around a central erbium(III) acceptor in a linear self-assembled cation (see **Figure 95**). This system presents several characteristics that can favour the ETU upconversion mechanism such as the high local concentrations of sensitisers, the choice of metals that gives a high efficiency for the Cr-Er energy transfer, and the wrapping of the helical ligand strands around the metal ion that protects them from the solvent.

Principal publication and authors
L. Aboshyan-Sorgho (a), C. Besnard (b), P. Pattison (c,d), K.R. Kittilstved (e), A. Aebischer (f), J-C. G. Bünzli (f), A. Hauser (e) and C. Piguet (a), *Angew. Chem. Int. Ed.* **50,** 4108–4112 (2011).
(a) Department of Inorganic, Analytical and Applied Chemistry. University of Geneva (Switzerland)
(b) Laboratory of Crystallography, University of Geneva (Switzerland)
(c) Laboratory of Crystallography Ecole Polytechnique Fédérale de Lausanne (Switzerland)
(d) Swiss Norwegian Beamline (SNBL), ESRF
(e) Department of Physical Chemistry University of Geneva (Switzerland)
(f) Laboratory of Lanthanide Supramolecular Chemistry Ecole Polytechnique Fédérale de Lausanne (Switzerland)

The minimum prerequisite for the generation of upconversion luminescence by a material is the existence of two metastable excited states, the first serving as an excitation reservoir, and the second as the emitting state. Different possible processes of up-conversion have been described [2], the two most common being excited-state absorption (ESA) and energy transfer upconvertion (ETU). ESA is a single ion mechanism which involves two sequential absorption processes. In the ETU process, at least two closely spaced ions are required. A sensitiser, which is excited to an intermediate excited state, transfers its energy to a neighbouring chromophore called acceptor, also in an intermediate excited state, promoting it to the upper emitting level (**Figure 95**). The existence of several excited states located between the ground state and the target excited state in lanthanide complexes makes them good candidates for such an upconversion mechanism, although it has long been thought that the vibrational oscillation of the organic ligands would quench this process for trivalent lanthanide ions [3]. However, with the development of the supramolecular chemistry of lanthanide complexes, using specially designed ligands, assemblies can be made

The structure of such highly paramagnetic slow-relaxing complexes is difficult to assess without the use of X-ray diffraction. NMR and EPR techniques are difficult to

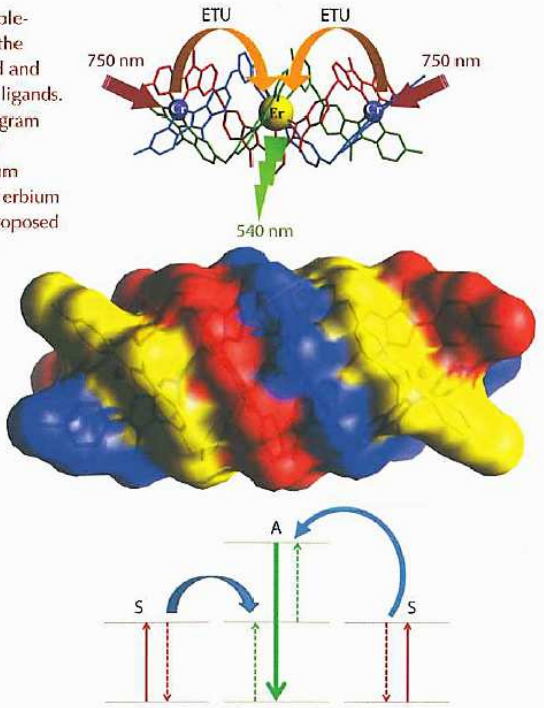

Fig. 95: The molecular triple-metallic complexes with the three metal atoms aligned and wrapped by three helical ligands. The simplified energy diagram shows the energy transfer between the two chromium atoms (sensitiser) and the erbium atom (acceptor) for the proposed ETU mechanism.

References
[1] D.H. Kim and J.U. Kang in *Microscopy: Science, Technology, Applications and Education* **1**, 571-582 (2010).
[2] F. Auzel, *Chem. Rev.* **104**, 139–173 (2004).
[3] C. Reinhard *and* H.U. Güdel, *Inorg. Chem.* **41**, 1048–1055 (2002).

use in these systems: NMR suffers from large line widths due to chromium(III) and EPR suffers from complications due to zero-field splitting, TIP effects and large line widths due to erbium(III). But as this compound crystallises with two complexes in the asymmetric unit, the unit-cell is large (volume 47200 Å^3). Moreover, disordered solvent molecules occupy channels inside the crystal, and the diffraction data from conventional sources in our laboratory were of poor quality. The higher quality of the data obtained from **BM01A**, the Swiss-Norwegian beamline, allowed us to unambiguously solve the structure and proved the organisation of the molecule.

The carefully chosen molecular design permitted green emission to be observed upon NIR irradiation of the sample, characteristic of the Er($^4S_{3/2} \rightarrow {}^4I_{15/2}$) transition. This first example of upconversion in an isolated molecular complex opens a new playground for synthetic chemists. New molecular designs connecting three Cr ions to the Er ion could for instance lead to unprecedented molecular three-photon upconversion luminescence.

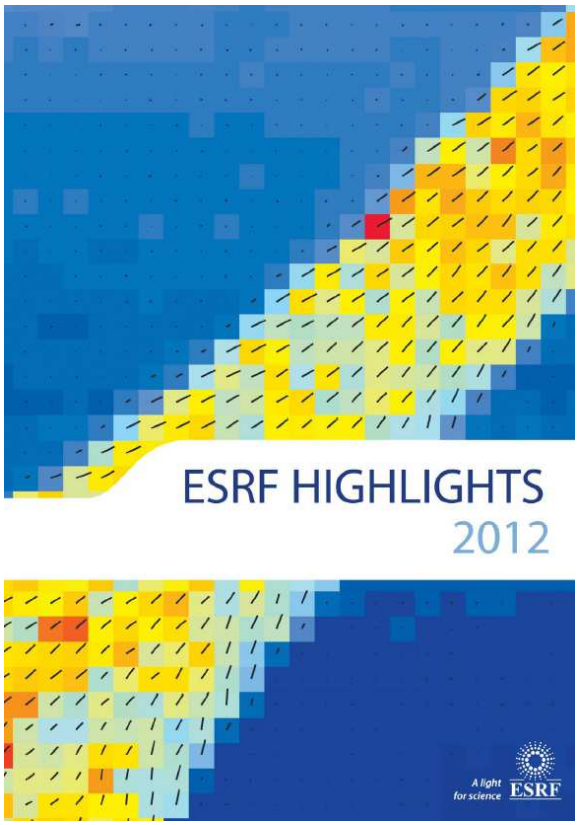

Microscopic and mesoscopic structure of functional perovskite ferroelectrics

Piezoelectric materials change their physical dimensions under application of an electric voltage and generate voltage under mechanical stress. Today they are widely used as sensors and actuators in various industries. In general, the most efficient piezoelectrics are mixed perovskites with composition close to the so-called morphotropic phase boundary (MPB). Near the MPB the ferroelectric phases of different symmetry have nearly the same energy and are separated by a rather small potential barrier. As a result, the different states can be easily switched by a small electrical or mechanical signal providing high electromechanical coupling. The exact structure and switching mechanisms are, however, challengingly complex and not yet understood. We combine diffuse and inelastic X-ray scattering experiments to reveal the character of structural heterogeneity in the most extensively used MPB piezoelectric – PZT.

Lead zirconate-titanate $PbZr_{1-x}Ti_xO_3$ (PZT) holds about 80% of the piezoelectric market. It is also a model system for studying the MPB phenomenon, which is observed for compositions when x is

Principal publications and authors
R.G. Burkovsky (a,b),
Y.A. Bronwald (a),
A.V. Filimonov (a), A.I. Rudskoy (a),
D. Chernyshov (c), A. Bosak (b),
J. Hlinka (d), X. Long (e),
Z.-G. Ye (e) and S. Vakhrushev (f,a),
Phys. Rev. Lett. **109**, 097603 (2012).
(a) St. Petersburg State Polytechnical University (Russia)
(b) ESRF
(c) SNBL at ESRF (France)
(d) Institute of Physics, Academy of Sciences of the Czech Republic, Prague (Czech Republic)
(e) Department of Chemistry and 4D LABS, Simon Frazer University, Burnaby (Canada)
(f) Ioffe Physical-Technical Institute, St. Petersburg (Russia)

around 0.48. Many diffraction studies have been devoted to understanding the structure of PZT near the MPB, but despite these efforts, the results and their interpretation remain controversial **[1]**. This is mainly due to the fact that diffraction studies reveal in almost all cases a structure, which is more complex than the single phase long-range ferroelectric order. The real microscopic structure can be studied effectively by analysing the scattering outside Bragg peaks by diffuse and inelastic scattering methods. We used these methods at beamlines **BM01A** and **ID28**, respectively. PZT single crystals of sufficient size and quality were grown at the Simon Frazer University (Canada).

Our diffraction measurements reveal the appearance of strong anisotropic diffuse scattering around Bragg spots (**Figure 47 a,c**) at temperatures just below the transition between two different ferroelectric phases (about T = 430 K). The observed scattering does not correspond to the polarisation fluctuations near the phase transition because it is absent on the high-temperature side of the ferroelectric-ferroelectric transition and also near the ferroelectric-paraelectric transition (about T = 663 K). Consequently, we have to assume another mechanism, which takes into account some structural inhomogeneity.

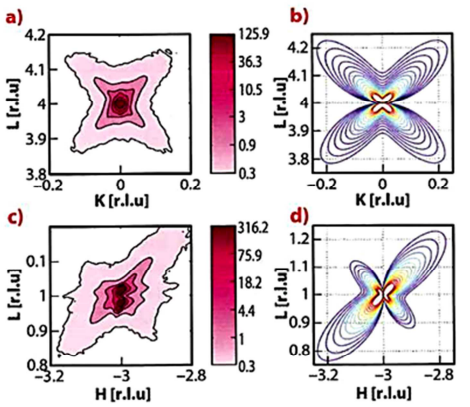

Fig. 47: Experimental diffuse scattering maps (a,c) and corresponding calculations (b,d).

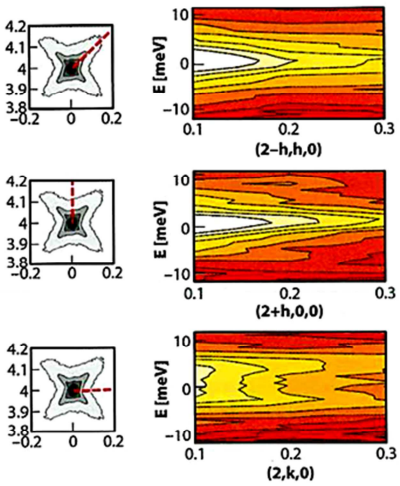

Fig. 48: Inelastic X-ray scattering maps along the three key directions of the (0 0 2) Brillouin zone.

To further understand the origin of diffuse scattering we used inelastic X-ray scattering (IXS). This technique allows static and dynamic components of diffuse scattering to be disentangled due to the meV energy analysis of the scattered photons. **Figure 48** schematically shows the IXS intensity maps along the inspected directions in reciprocal space. We observe strong quasielastic scattering (centred at zero energy-transfer) in diagonal and longitudinal directions, while in transverse directions the scattering is almost purely inelastic. Therefore, the observed diffuse scattering (**Figure 47a**) is a superposition of two contributions: one is due to phonons and the other one is due to static deviations from long-range order. The important feature of this second component is the absence of any intensity along the transverse direction. To reproduce this feature with models by considering the diffuse scattering as a Fourier image of real-space objects or 3D correlators was not possible. In contrast, it is consistent with Huang scattering – scattering due to inhomogeneous deformations of the lattice. More specifically, we note a very good agreement (**Figure 47 b,d**) with experimental data when the deformations are modelled as being due to tetragonal-symmetry point defects in a matrix that is nearly cubic. From the anisotropy of the diffuse scattering, it can be deduced that these defects produce very small volume strain due to the specific ratio between tensile strain along the main tetragonal direction and compressive strain along the two other directions. The emerging physical picture behind this model assumes that small clusters of the tetragonal phase remain in the matrix of the new average structure below the ferroelectric-ferroelectric phase transition temperature. In this model

we associate the diffuse scattering with the scattering by the matrix surrounding the clusters (not with the scattering by the clusters themselves, which are too small for direct observation) because the matrix is deformed on a larger, mesoscopic scale.

Last, but not least, the observed morphotropic PZT diffuse scattering appears at first sight to be very similar in shape to that of relaxor ferroelectrics **[2]** – a different and special class of disordered perovskites. However there are clear topological differences with respect to the relaxor case – in (0 0 L) Brillouin zones of PZT the transverse diffuse scattering component is suppressed, while for diffuse scattering in relaxors, the minimum of intensity appears along the longitudinal direction. This forms a solid basis for the assumption that the origin of diffuse scattering in these two classes of materials is also different. We believe that the present work on PZT will further stimulate the development of a common understanding of disorder phenomena in functional perovskite ferroelectrics.

References
[1] J. Kreisel, B. Noheda and B. Dkhil, *Phase Transitions* **82**, 633 (2009).
[2] A. Bosak, D. Chernyshov, S. Vakhrushev and M. Krisch, *Acta Crystallographica* **A68**, 117 (2012).

Principal publication and authors
E. Verheyen (a), L. Joos (b), K. Van Havenbergh (c), E. Breynaert (a), N. Kasian (a,d), E. Gobechiya (a), K. Houthoofd (a), C. Martineau (e), M. Hinterstein (f), F. Taulelle (e), V. Van Speybroeck (b), M. Waroquier (b), S. Bals (c), G. Van Tendeloo (c), C.E.A. Kirschhock (a) and J.A. Martens (a), *Nat. Mater.* **11**, 1059–1064 (2012).
(a) Center for Surface Chemistry and Catalysis, KU Leuven (Belgium)
(b) Center for Molecular Modeling, Ghent University (Belgium)
(c) Electron Microscopy for Materials Science, University of Antwerp (Belgium)
(d) L.V. Pisarzhevsky Institute of Physical Chemistry, National Academy of Sciences of Ukraine, Kyiv (Ukraine)
(e) Tectospin, Institut Lavoisier, UMR 8180 Université de Versailles (France)
(f) Institut für Werkstoffwissenschaft, Technische Universität Dresden (Germany)

Design of zeolite by inverse sigma transformation: Cut and paste zeolites

Zeolites are crystalline microporous aluminosilicates which consist of corner-sharing TO_4 tetrahedra. They are workhorses in industry for adsorption, separation and catalysis. Heteroelements are often inserted to enhance desired properties such as catalytic activity and selectivity. The introduction of germanium however results in stability problems.

Germanosilicate IM-12 zeolite (UTL topology) consists of dense silicate layers connected by double-four rings (D4Rs), the preferential location of germanium (**Figure 138**). The systematic instability of the UTL zeolite can be used to harvest building units that can be rearranged to transform UTL zeolite into a new and stable zeolite. Acid leaching removes the germanium from the UTL framework while preserving the dense silicate layers and reconnects these layers to form new zeolite topologies –COK-14 or COK-14. –COK-14 is a new all-silica interrupted framework topology with a two-dimensional channel system and interconnecting 8-, 10- and 12-membered rings (**Figure 138**). Upon drying in the absence of water, silanol condensation takes place and COK-14 is formed (**Figure 138**). The transformation from UTL zeolite to COK-14 involves the systematic removal of one layer of T-atoms and as such is the first experimentally observed inverse sigma transformation.

To verify if a true inverse sigma transformation occurred, an intermediate state was captured named Ge-COK-14. This sample was synthesised by reducing transformation time. ^{29}Si-NMR and ^{1}H-NMR indicated this sample contained Q^3 silicon environments, associated with silanol groups, while still having Si-O-Ge bonds. Approximately 50 wt% of the original germanium content was still present in Ge-COK-14. High-resolution powder X-ray diffraction data and X-ray absorption spectra for Ge-COK-were collected at room temperature at beamline BM01B (the Swiss Norwegian Beamline SNBL) in collaboration with beamline BM26 (DUBBLE) (**Figure 139**). Indexing of the powder pattern of Ge-COK-14 resulted in a unit cell of a = 24.43 Å, b = 13.90 Å, c = 12.28 Å and a monoclinic angle of 108.97° compared to a = 24.64 Å, b = 13.92 Å, c = 12.26 Å and β = 109.20° for –COK-14 and a = 29.00 Å, b = 13.98 Å, c = 12.45 Å and β = 104.91° for the parent UTL zeolite. This indicated that Ge-COK-14 already had the interlayer spacing of –COK-14 but still contained germanium. Ge K-edge EXAFS spectra revealed the local environment

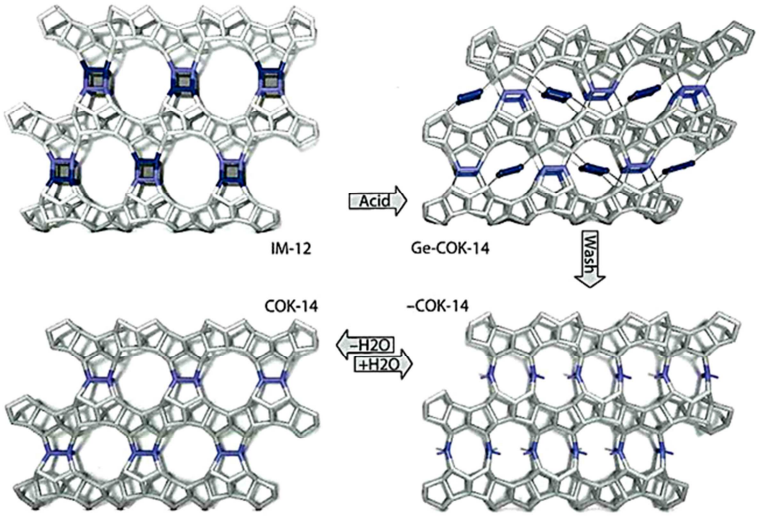

Fig. 138: Acid leaching of IM-12 zeolite can dislodge the germanate four-ring (dark blue) and shift it into the channels of the contracted framework of Ge-COK-14. Further acid leaching fully eliminates the germanate four-ring resulting in the interrupted (-COK-14) or fully condensed framework (COK-14) depending on the conditions.

and coordination of Ge in Ge-COK-14 (**Figure 139**). Each Ge atom had two Ge neighbours at 3.2 Å. A combination of HRXRD and Ge-K-edge EXAFS measurements allowed the structure of Ge-COK-14 to be unravelled (**Figure 138**, **Figure 139**). In this sample, germanium was present as a germanate four-ring in the position that would later become the 12-membered ring of COK-14. Ge-K-edge EXAFS measurements of the parent UTL zeolite revealed this germanate four-ring was already present (**Figure 138**).

Acid leaching removes the germanate four-ring from the UTL zeolite and shifts it into the channels of Ge-COK-14. Prolonging the transformation and washing leads to full elimination of germanium and results in the new zeolite frameworks –COK-14 and COK-14 (**Figure 138**). The COK-14 zeolite family is a valuable addition to the all-silica large-pore zeolite types. More new zeolites with attractive pore architectures may be obtained by this inverse sigma transformation approach.

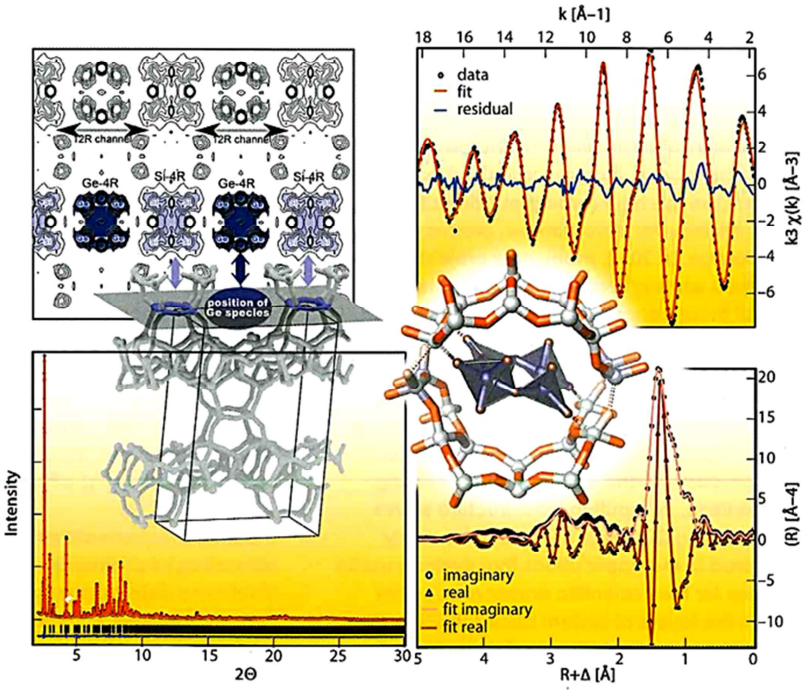

Fig. 139: Rietveld refinement (bottom left), observed electron density (upper left) and fitted EXAFS data (right) of Ge-COK-14. EXAFS analysis was based on the inserted fragment from Rietveld refinement. Inset on the left indicates the shown plane of observed electron density.

Direct Observation of Catalyst Behaviour Under Real Working Conditions With X-ray Diffraction: Comparing SAPO-18 and SAPO-34 Methanol to Olefin Catalysts

David S. Wragg[a],* Duncan Akporiaye[b] and Helmer Fjellvåg[a]

[a]*inGAP Centre for Research Based Innovation, Centre for Materials Science and Nanotechnology and Department of Chemistry, University of Oslo, P.O. box 1033 Blindern, N-0315 Oslo, Norway*

[b]*SINTEF Materials and Chemistry Forskningsvn 1, N-0314 Oslo, Norway*

The methanol to olefin (MTO) conversion process is an important route from cheap and potentially renewable feedstocks to high value chemical building blocks. The first commercial plants using the process are now coming on stream in China. Olefins (hydrocarbons containing double carbon to carbon bonds) can be converted into all kinds of chemical products, especially polymers. They are currently obtained mainly by distillation of oil. The MTO process is particularly effective for producing propylene (propene), the starting point for polypropylene which can be fabricated into anything from high strength plastic sheets to thermal underwear. The process is catalysed by small pore zeolites, and the most successful catalyst is the silicon substituted aluminium phosphate framework SAPO-34. This catalyst has excellent selectivity for propylene (many of the other catalysts produce a very wide product range making separation a major problem) but is quickly deactivated by coke- organic material developed from the reaction intermediates trapped inside the framework. This is remedied by repeated burning of the coke to regenerate the catalyst. SAPO-34 also suffers long term deactivation after many cycles of MTO and regeneration. The cause of this is not known [1]. It is vital to understand the catalytic process better in order to extend the lifetime of the catalyst. A longer lived catalyst would lead to significant cost reductions, for example it may allow MTO plants to move from the complex and costly recirculating fluidised bed reactors currently used to simple fixed bed systems as used in the methanol to gasoline process.

The MTO process has been developed in collaboration by UOP in America and Ineos (formerly Norsk Hydro) in Norway. Extensive research and development work on the process has been carried out at the University of Oslo, NTNU and SINTEF. Catalytic studies have revealed much about the mechanism of the reaction taking place inside the zeolite catalyst, however, until recently there had been no significant research into the behaviour of the catalyst itself during the process. Using the MAR2300 image plate system on BM01A of the SNBL we began to study the behaviour of SAPO-34 under MTO reaction conditions using the capillary flow cell developed by Norby [2]. The first results were published in 2009 [3, 4]. Using the the Rietveld method to analyse series of in situ XRD data we discovered significant changes in the crystal structure of SAPO-34 during the MTO process and adsorption of water and methanol. The main structural changes are focussed on the c-axis of the rhombohedral (hexagonal setting) unit cell which expands significantly during the MTO process.

SAPO-34 is not, however, the only small pore zeolite framework which is active for MTO conversion. Some publications have suggested that SAPO-18, a closely related structure, has superior properties as an MTO catalyst, especially in terms of lifetime.

We set out to study the behaviour of SAPO-18 in the MTO process and compare it to our earlier results on SAPO-34. The two structures are closely related. Both are built up from double six ring units (D6Rs), i.e. two connected rings of six tetrahedral Si/Al/P atoms linked by oxygen; which are arranged in identical layers. An A-A-A stacking of the layers gives SAPO-34 (International Zeolite Association framework type CHA) while and A-B-A sequence (with the B layer simply the A-type layer rotated by 180°) gives SAPO-18 (International Zeolite Association framework type AEI). The layers form structures with 8-ring windows (rings of 8 tetrahedral atoms linked by oxygen) and large internal cages. The ordering of the D6Rs is, however, slightly different [10]. This leads to two structures with the same framework density (number of tetrahedral atoms per 1000 Å3; 15.1 for both structures) but significantly different cage shapes (figure 1).
Data were collected on SAPO-18 (containing 8 % silicon) under MTO conditions on BM01A. The reaction was run for 3 hours at 450 °C and powder patterns were collected with a time resolution of 107 seconds. Mass spectrometry data were collected during the experiment. The PXRD data were refined using the Rietveld method with GSAS and TOPAS academic with both batch and parametric methods.

The unit cell of SAPO-18 is expands during the MTO process but to a smaller degree than SAPO-34 with the same silicon content. In contrast to SAPO-34 variations of similar magnitude are observed in all unit cell directions, leading to a 0.9 % volume

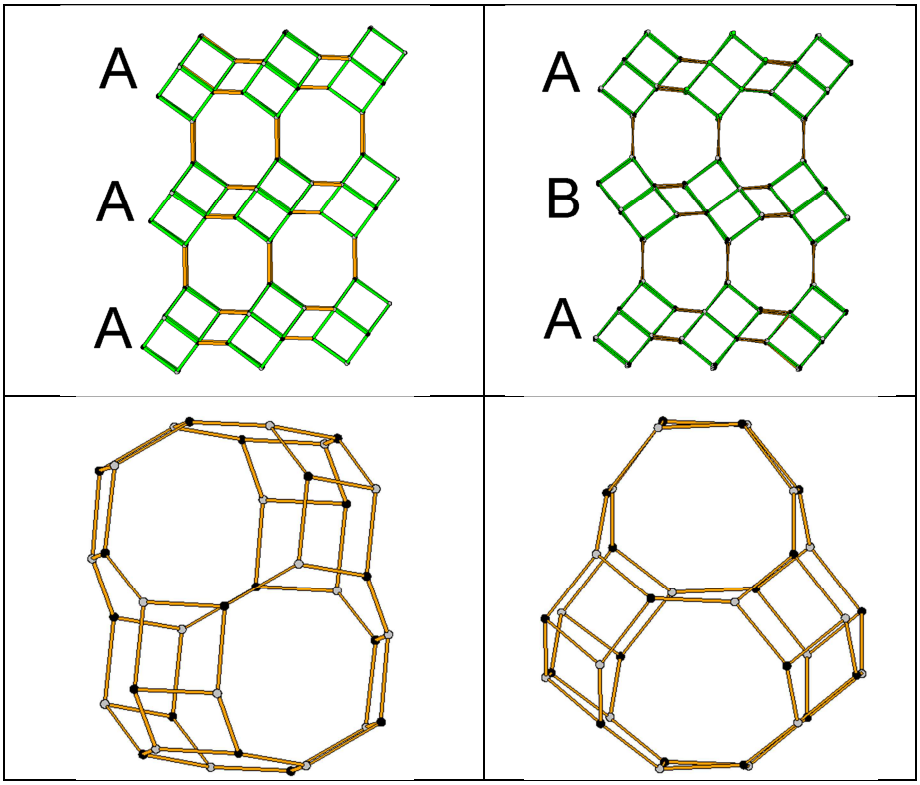

Figure 1. The structures of SAPO-34 (left) and SAPO-18 (right) showing the stacking schemes and resulting cages.

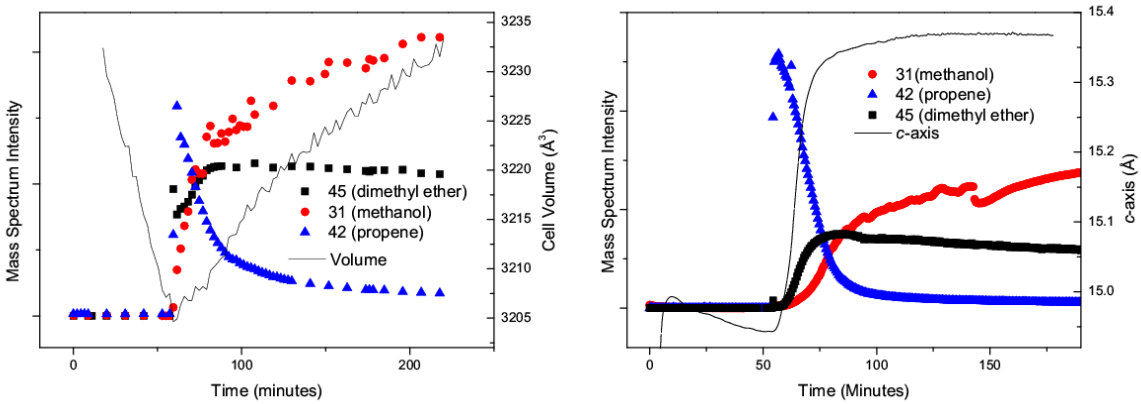

Figure 2. Unit cell expansion and mass spec data for SAPO-18 (left) and SAPO-34 (right).

expansion compared to 3 % for SAPO-34. There is no clear endpoint for the expansion of SAPO-18 which may reflect the longer active lifetime of this catalyst (figure 2).

Expansion in SAPO-34 during the MTO process is strongly correlated to the build-up of reaction intermediates inside the cages. Marcus et al compared the coke in SAPO-18 and SAPO-34 after the MTO process and showed that SAPO-18 tends to form larger polyaromatic species than SAPO-34 (pyrenes rather than phenanthrenes), this is explained by the shape of the cages in SAPO-18 allowing easier formation of the larger aromatics [5]. Even with pyrene trapped inside there is space in the SAPO-18 cage. This observation helps to rationalise both the smaller expansion observed by in situ X-ray diffraction and the extended activity: SAPO-34 fills with coke, expands, becomes blocked and deactivates. Due to its cage shape SAPO-18 does not fill, despite the larger coke molecules, and therefore need not expand.

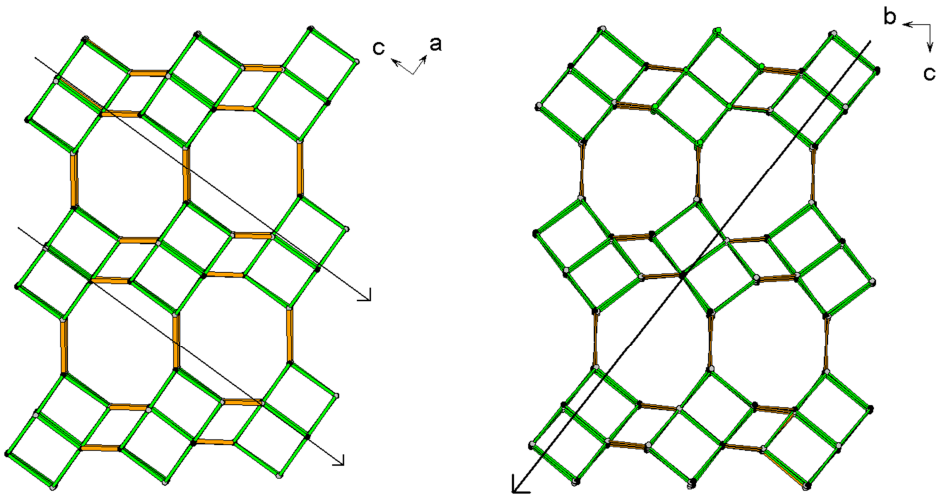

Figure 3. Comparison of the structures of SAPO-34 (left) and SAPO-18 (right) showing the arrangements of double six ring units (green).

We furthermore suggest that the structure of SAPO-18 may be more rigid than that of SAPO-34. In the latter the D6R units are all aligned in the same direction and the flexible four ring links allow the whole structure to expand easily in the c-direction. In SAPO-18 alternate cages are rotated by approximately 90° with respect to one another (figure 3); this means that changes to the size of the cages are restricted by the necessity of deforming the more rigid D6R units.

Plotting the change electron density in the cages per formula unit against reaction time shows a trend which matches the shape of the unit cell volume expansion curve (figure 4) as previously observed for SAPO-34. The level of electron density per formula unit in SAPO-18 is higher than that found for SAPO-34 supporting the theory that larger intermediates are present in SAPO-18.

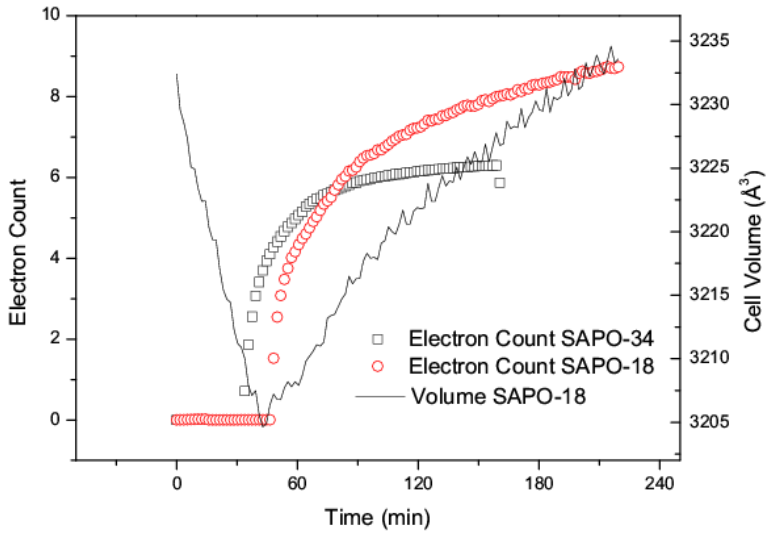

Figure 4. Volume expansion and cage electron counts for SAPO-34 and SAPO-18

This work has revealed that it is likely that the longer active lifetime of SAPO-18 compared to SAPO-34 is related to the differences in structural behaviour, with the cage shape and rigid framework delaying pore blocking.

References

[1] P. Barger, Methanol to Olefins (MTO) and Beyond, in: M. Guisnet, J.-P. Gilson (Eds.) Zeolite for Cleaner Technologies, Imperial College Press, London, 2002, pp. 239-260.
[2] P. Norby, J. Am. Chem. Soc., 119 (1997) 5215-5221.
[3] D.S. Wragg, R.E. Johnsen, M. Balasundaram, P. Norby, H. Fjellvåg, A. Grønvold, T. Fuglerud, J. Hafizovic, Ø.B. Vistad, D. Akporiaye, J. Catal., 268 (2009) 290-296.
[4] D.S. Wragg, R.E. Johnsen, P. Norby, H. Fjellvåg, Microporous Mesoporous Mater., 134 (2010) 210-215.
[5] D.M. Marcus, W. Song, L.L. Ng, J.F. Haw, Langmuir, 18 (2002) 8386-8391.

Publication

D. S. Wragg, D. Akporiaye and H. Fjellvåg, Journal of Catalysis, (2011), **279**, 397-402.

Ionothermal Synthesis and Structure Analysis of an Open-Framework Zirconium Phosphate with a High CO_2/CH_4 Adsorption Ratio

Lei Liu[(a)], Jiangfeng Yang[(a)], Jinping Li[(a)], Jinxiang Dong[(a)], Dubravka Sisak[(b)], Marisa Luzzatto[(b)], and Lynne McCusker[(b)]

(a) Research Institute of Special Chemicals, Taiyuan University of Technology, Taiyuan, Shanxi (P.R. China)
(b) Laboratorium für Kristallographie, ETH Zürich, Zürich (Switzerland)

Zirconium phosphate materials have been investigated extensively because of their potential for application in the fields of ion-exchange, catalysis, photochemistry, and biotechnology. Most studies of these materials have focused on the two layer compounds α-$Zr(HPO_4)_2 \cdot H_2O$ and γ-$ZrPO_4$-$(H_2PO_4) \cdot 2H_2O$ and their derivatives, which are obtained by post-synthesis processing techniques (for example ionexchange, intercalation, or grafting). The main reason most other zirconium phosphate materials have been neglected can probably be attributed to their poor thermostability.They have generally been synthesized using organic amines as structure-directing agents in a hydro-/solvothermal procedure. Of these templated zirconium phosphate materials, those with framework (rather than layer) structures tend to have a higher thermostability, but they are difficult to synthesize using this conventional synthetic approach. In fact, only two open-framework structures have resulted from these efforts. Unfortunately, neither is stable to the removal of the occluded organic species by calcination, so they cannot be used as microporous materials for gas adsorption or separation, or for shape-selective catalysis.

Recently, our group reported the ionothermal synthesis of a zirconium phosphate using a deep-eutectic solvent (DES), which consisted of carboxylic acid and quaternary ammonium salts. The resulting framework structure was found to depend on the structure and steric effect of the quaternary ammonium cation. Herein, we combined ethylammonium chloride and oxalic acid to form a DES with a melting point below 100ºC, and then used it to synthesize a novel open-framework zirconium phosphate, $C_2H_7NH)_8(H_2O)_8][Zr_{32}P_{48}O_{176}F_8(OH)_{16}]$ (denoted hereafter as ZrPOF-EA). The crystal structure of ZrPOF-EA (Fig.1) was solved from high resolution powder diffraction data collected on the Swiss–Norwegian Beamline, BM01B, in the orthorhombic system (a=6.165Å, b=19.955Å, c=37.062Å) and reflection intensities were extracted assuming the space group P*mc*2_1. These data were used as input to the powder charge-flipping (pCF) algorithm in the program Superflip for structure solution. The best electron density map from the first pCF run was used as a seed to generate the starting phase sets for the second run, and the best of the resulting maps was interpreted to yield the positions of all 16 zirconium, 23 of the 24 phosphorus, and 55 of the 77 oxygen atoms. A series of difference electron density maps led to the location of the missing phosphorus atom, the terminal oxygen atoms, and the non-framework species. Atoms bridging between two zirconium atoms were assigned as fluorine. During the course of the refinement, it became apparent that most of the framework atoms followed the symmetry of the higher space group P*bam*, so refinement was completed in that space group even though it meant that the terminal P-OH groups and the organic cations were disordered. This refinement, with 8 zirconium, 12 phosphorus, 40 oxygen, 2 fluorine, 2 water, and 3 ethyl

ammonium ions in the asymmetric unit, converged with the R values R_F=0.038, and R_{wp}=0.170 (R_{exp}=0.171).

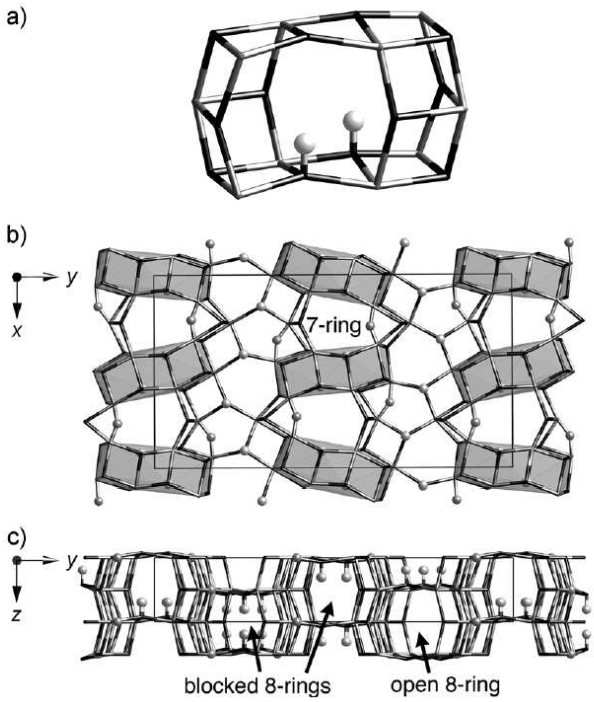

Figure 1. ZrPOF-EA framework structure showing a) the characteristic [$4^{14}8^2$] unit, b) the projection along the *c* axis with the [$4^{14}8^2$] units highlighted, and c) the projection along the *a* axis. Bridging O atoms have been omitted for clarity. Terminal O atoms and bridging F atoms are shown as balls, Zr gray, and P black.

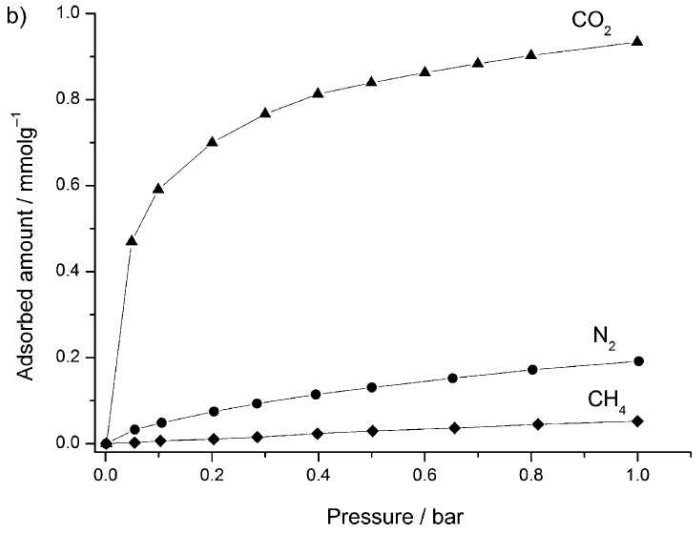

Figure 2. Adsorption isotherms of CO_2, N_2, and CH_4 for ZrPOF-EA at 25ºC, in the low-pressure range (0–1 bar).

In ZrPOF-EA, the oval 7- and 8-ring windows have dimensions of about 4.0 x 3.0 Å and 3.9 x 3.2 Å, respectively. To establish its adsorption properties, CO_2, N_2, and CH_4 adsorption experiments were carried out on an intelligent gravimetric analyzer (IGA-001, Hiden Isochema) at 25ºC. Before each adsorption experiment, the activated ZrPOF-EA was outgassed at 300ºC under vacuum for 10 h. From the adsorption isotherms shown in Fig.2, it is evident that the adsorption capacity for CO_2 is markedly higher than that for CH_4, with a CO_2/CH_4 adsorption ratio ranging from 67.2 at 0.2 bar to 17.3 at 1 bar. The selective adsorption of CO2 may be a result of the complicated pore structure and the polar hydroxy groups directed into the pore channels. The small 7- and 8-ring pore openings allow CO_2 molecules (3.3 Å kinetic diameter) to enter the channels, but block the larger CH_4 molecules (3.8 Å kinetic diameter). Furthermore, the low N_2 adsorption capacity indicates that even the intermediate-sized N_2 (3.6 Å kinetic diameter) has difficulty in entering the pores, leading to a CO_2/N_2 adsorption ratio ranging from 12.2 at 0.2 bar to 4.9 at 1 bar.

One of the applications of CO_2 separation technologies is in the upgrade of biogas to pure or more concentrated methane. Biogas, which is essentially a mixture of CO_2 (ca. 25–45%) and CH_4, is a very important source of renewable methane produced by the anaerobic digestion of waste materials. Although ZrPOF-EA has a relatively low adsorption capacity, its high CO_2/CH_4 adsorption ratio may find industrial application in membrane separation technology for upgrading such natural gas.

Principal publication

Lei Liu, Jiangfeng Yang, Jinping Li, Jinxiang Dong, Dubravka Sisak, Marisa Luzzatto, and LynneB. McCusker, *Angew. Chem. Int. Ed.* 2011*,* **50***, 8139 –8142.*

The influence of X-rays on different redox states of crystalline myoglobin.

Hans-Petter Hersleth and K. Kristoffer Andersson
Dept.of Biosciences, University of Oslo, PO Box 1066 Blindern, 0316 Oslo, Norway

X-ray induced radiation damage of protein crystals is well known to occur even at cryogenic temperatures, and redox active sites like metal and radical sites seem especially vulnerable for these radiation-induced reductions. It is essential to know correctly the oxidation state of metal-ion sites in protein crystal structures to be able to interpret the structure-function relation. To better understand how metalloproteins are influenced by X-rays during crystallographic data collection we have chosen to study different redox states generated in the reaction between myoglobin (Mb) and peroxides (coloured red in *Fig. 1*). These different states have characteristic light absorption spectra in the 450-700 nm, and can therefore be monitored by single-crystal online microspectrophotometry (*Fig. 1*). The radiation-influenced structures of these states have previously been determined at SNBL and ESRF (*Fig. 2*).

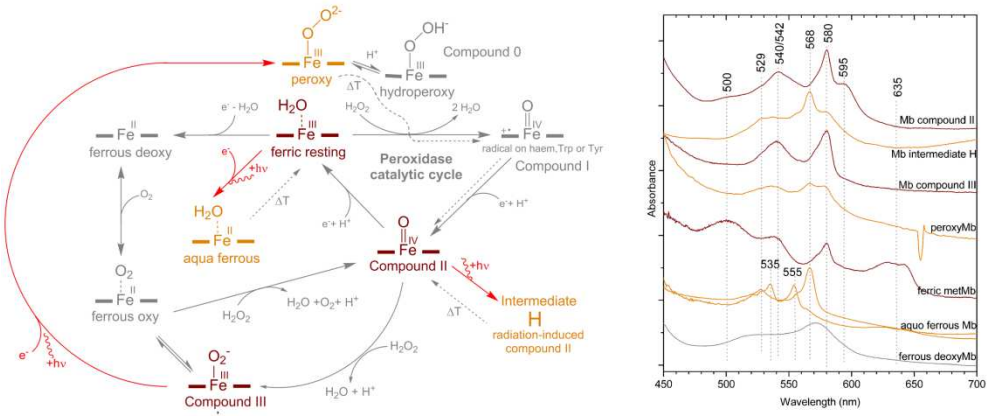

Figure 1: Reaction scheme showing the different Mb redox states with corresponding single-crystal light absorption spectra.

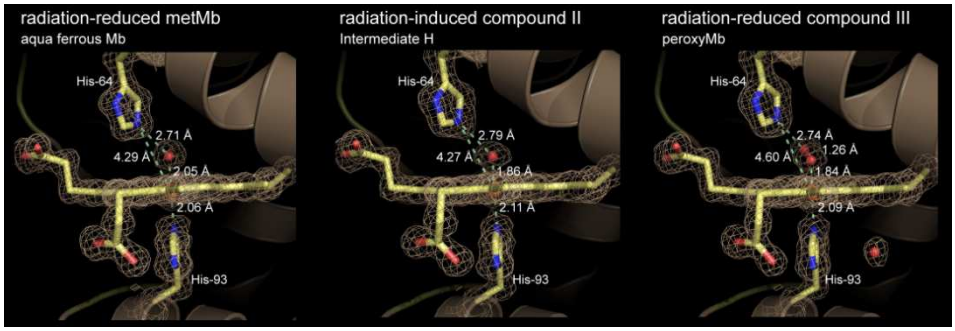

Figure 2: Structures of radiation-influenced states of Mb (PDB codes: 2V1I, 2V1E, 2VLX)

In this study, we have in detail investigated the impact that X-rays have on these different oxidation states of Mb, to understand how fast these states are influenced, and to determine how much X-rays you can use before the different states are too heavily influenced/reduced by X-rays. In order to investigate how the lifedoses vary among different oxidation states of metalloproteins we have systematically analysed

the effect X-rays have on the ferric Fe^{III} metMb, compound II Fe^{IV}=O ferrylMb and Mb compound III Fe^{III}-O_2^- states with single-crystal spectroscopy.

Fast X-ray influence of the ferric metMb – determination of lifedose

The metMb state have characteristic light absorption peaks at 500, 540, 581 and 635 nm, while the radiation-reduced state have the most dominant peaks at 529 and 568 nm. *Fig 3* shows that the influence/reduction begins immediately; from the first X-ray photon that hits the crystal. The appearance of the 568 nm peak is clearly seen after an absorbed dose of only 0.0053 MGy (*Fig. 3*; middle).

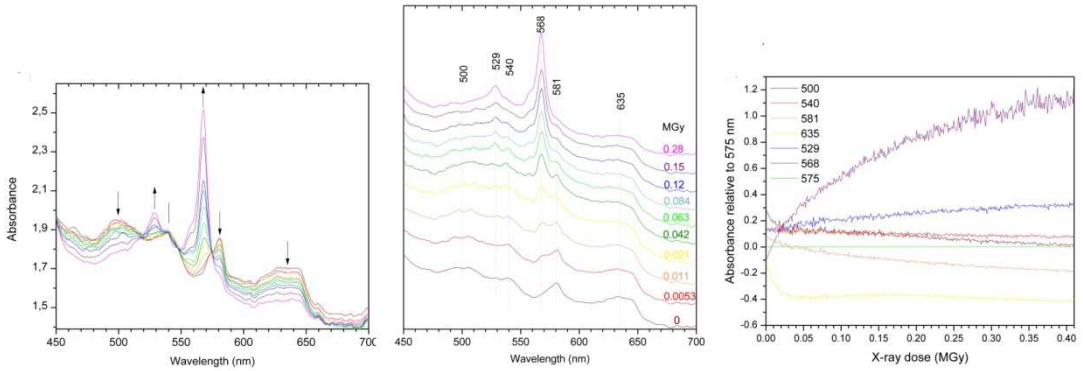

Figure 3: Single-crystal light absorption spectra of a ferric Fe^{III} metMb: (left) overlay of spectra at selected time/dose points, (middle) selected spectra at increasing time/dose points; (right) propagation of the different peaks of metMb and the radiation-induced state relative to the isosbestic point at 575 nm.

To determine a suitable lifedose, which can be used for composite data collection strategies, is not trivial. Remaining of ~90% of the initial state might be a suitable limit. However, the background is considerably increased by the solvated electrons during the first seconds of irradiation. This elevation reaches a maximum and then decays slowly. To remove the background effect, the absorbance of the different peaks have in *Fig. 3* (right) been retracted the absorbance of the isosbestic point at 575 nm. This result in a figure showing the increase and decrease of the different peaks with respect to X-ray exposure/absorbed X-ray dose (*Fig. 3*; right). The 568 and 529 nm peaks of the radiation-induced state increase, especially 568 nm, while the 500, 540, 581 and 635 of metMb decrease slowly. The lifedose has been taken to be the dose it takes for the original state to decay to 90%. To be able to calculate this value, we have taken the absorbance at 581 nm and retracted the absorbance at the closest isosbestic point at 575 nm to correct for the background. The decrease of this peak to 90% has been determined to be ~0.01 MGy (equals ~12 seconds of exposure at ID14-2 with 37.7% transmission).

The radiation-reduced ferric metMb state is believed to be an aquo or hydroxy ferrous state. An interesting observation is that an annealing of this state, seems to regenerate the original metMb state as observed with both light absorption and Raman spectroscopy. The single-crystal off-resonant Raman spectrum of ferric metMb is shown in *Fig. 4*, exhibiting the characteristic ferric haem modes (e.g. the ν_4 oxidation state marker at 1371 cm^{-1}). After X-ray irradiation corresponding to a dose of 1.4 MGy, the Raman signal is much weaker than for the resting state (*Fig. 4*). For this radiation-induced ferric metMb state most of the haem modes have diminished, moved and/or become more undefined. After a short annealing, several of the haem modes of the ferric metMb state reappear.

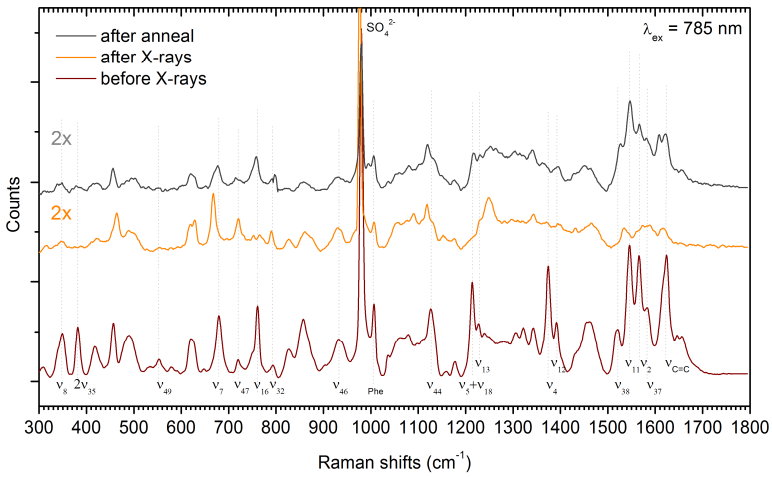

Figure 4: Single-crystal off-resonant Raman spectra of a ferric Fe^{III} metMb crystal: (dark red) before irradiation with X-rays, (orange) after irradiating with X-rays corresponding to an absorbed dose of ~1.4 MGy, and (grey) after annealing.

Influence on the different redox states of Mb – determination of lifedoses

The fast influence/reduction observed for metMb is also observed for the compound II Fe^{IV}=O ferrylMb and Mb compound III Fe^{III}-O_2^- (*Fig. 5*).

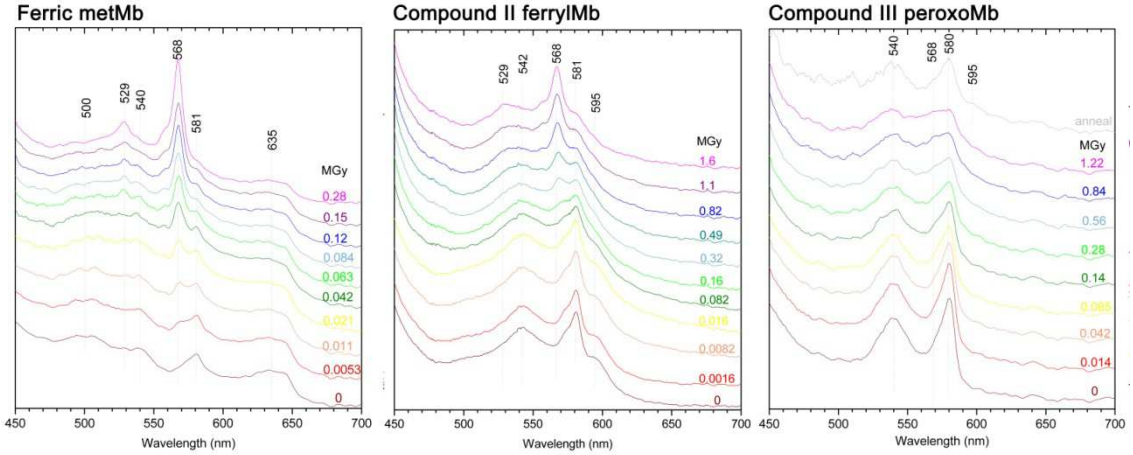

Figure 5: Selected single-crystal light absorption spectra of different redox states of Mb with increasing time/dose points: (left) ferric Fe^{III} metMb; (middle) compound II Fe^{IV}=O ferrylMb; (right) Mb compound III Fe^{III}-O_2^-.

The characteristic ferrylMb peaks at 542, 581 and 595 are slowly decreasing, while the peaks for the radiation-reduced state gradually appears at 529 and 568 nm with well defined isosbestic points at 528, 556 and 572 (*Fig. 5*; middle). A calculation of the lifedose in a similar way as for metMb gives doses of ~0.02-0.03 MGy (90% of 581 nm). The lifedose estimations therefore indicate the striking fact that the Compound II ferrylMb is not as easily reduced as the lower oxidation state of ferric metMb. A time/dose monitoring with light absorption is therefore needed for each individual oxidation state. The fact that it is the same peaks that appears for both ferricMb and ferrylMb raise the question if it is a real and similar reduction to aquo ferrous of both states, or if it is some part of the haem moiety that is reduced similarly in the two states. However, the increase of the 568 nm differs between the ferric and ferryl states. The crystal structures of the radiation-reduced states of metMb and

ferrylMb show also a different Fe-O distance, 2.05 and 1.84 Å, respectively, demonstrating that these radiation-induced states cannot be identical with respect to the iron (*Fig. 2*).

For Mb compound III Fe^{III}-O_2^- the characteristic compound III peaks at 540 and 580 nm decrease with increasing dose (*Fig. 5*; right). The 568 nm peak increase very slowly for this state, compared to the ferric and ferryl states. The estimation of the lifedose for this state results in quite similar values: ~0.02 MGy (90% of 580 nm) Table1,

Table 1

Redox state	Lifedose*
Ferric Fe^{III} metMb	~ 0.01 MGy
Compound II $Fe^{IV}O$ ferrylMb	~ 0.02 MGy
Compound III Fe^{III}-O_2^- peroxoMb	~ 0.02 MGy

***** When 90% of the original state remains: Dose at which the 581 nm peak has fallen to 90% of the initial absorbance relative to the isosbestic point

Summary

All the three Mb states (ferric Fe^{III} metMb, compound II Fe^{IV}=O ferrylMb and Mb compound III Fe^{III}-O_2^-) are influenced / reduced by the X-rays used for structure determination. How fast these changes occur vary slightly between the different crystalline states. However, all these lifedoses are on a much shorter timescale than the lifedoses used for protein crystals in general. The lifedose / Hendersson limit for a "normal" protein crystal (without a redox site) is ~20 MGy. The lifedoses we have estimated here for obtaining the structure of unreduced Mb redox states are therefore about 1000 times less than the general Hendersson limit. In general, we would argue that monitoring of a spectroscopic property as a function of time / dose should always accompany the structure determination of a metalloprotein to confirm its correct oxidation state.

Acknowledgements.

The investigation has been supported by funding from the Norwegian Research Council: grant 177661/V30, 214239/F20 and 218412/F50 (to K.K.A) and travel grant 138370/V30. We gratefully acknowledge the ESRF (MX765, MX885) for providing beam time with online microspectrophotometer, the Swiss-Norwegian Beam Line (SNBL) at ESRF (01-02-784) for providing beam time with online Raman spectroscopy, and SLS (20091133) for providing beamtime with online microspectrophotometer. We thank the team at the MX-Beamlines for the help with the online microspectrophotometer setup at ID14-2, the team at SNBL for help with the online Raman setup and Wouter van Beek for help and discussion, and the team at X10SA for help with the on-axis online microspectrophotometer.

Publication:

Hersleth, H.-P. & Andersson, K.K. (2011) How different oxidation states of crystalline myoglobin are influenced by X-rays. *Bichim. Biophys. Acta, Proteins Proteomics*. **1814**, 785-796.

The luminescence of $Na_xEu^{3+}_{(2-x)/3}MoO_4$ scheelites depends on the number of Eu-clusters occurring in their incommensurately modulated structure.

A.Arakcheeva[(a)], D.Logvinovich[(a,b)], G.Chapuis[(a)], V.Morozov[(c)], S.Eliseeva[(c)], J.-C.Bünzli[(d,e)], P.Pattison[(a,f)]

(a) Laboratoire de cristallographie, Ecole Polytechnique Federale de Lausanne, 1015 Lausanne, Switzerland.
(b) ETH Honggerberg, Laboratorium fur Kristallographie, 8093 Zurich, Switzerland
(c) Department of Chemistry, Moscow State University, 119991 Moscow, Russia
(d) Institute of Chemical Sciences and Engineering, Ecole Polytechnique Federale de Lausanne, 1015 Lausanne, Switzerland
(e) WCU Center for Next Generation Photovoltaic Devices, Korea University, Jochiwon, Republic of Korea
(f) Swiss-Norwegian Beam Lines at ESRF Grenoble BP-220, 38043, France

Scheelite related compounds (SRCs) with general formula $M_n(XO_4)_m = M_n/m(XO_4)$ cover a broad spectrum of compositions, with M being either a single element or a combination of up to three cations, which can be alkaline elements, Ca, Sr, Pb, Ba, Zn, Cd, In, Ga, Tl, Ln, Y and Bi, while X is Mo, W, Nb, V, Ta or, possibly, a combination thereof. They are highly stable and their preparation by solid-state reaction is easy so that scheelites are found in many industrial applications, including solid oxide fuel cells and photocatalysts. The chemical composition and size of the particles are important factors affecting the luminescence of SRC phosphors. Influence of the crystal structure on the luminescence properties has been discussed for some SRCs. However, this aspect is usually ignored because only statistical distributions can be derived for different M-cations by conventional crystallographic methods. On the other hand, application of the (3 + 1)-dimensional symmetry concept shows that the entire family of compositionally different SRCs can be described from a unique model of modulated structures, which is characterized by a fully ordered distribution of different cations in the M subset.

The vast majority of the published SRCs exhibit the stoichiometry $M : XO_4 = m/n = 1$, leaving no possibilities for vacancies in the M subset. Only charge neutrality limits the m/n ratio in the modulated structure model. Hence, this model allows one to predict SRCs with completely ordered structures within a wide and continuous range of compositions. The modulated structures can be identified by the presence of additional satellite reflections in the lower angle part of XRD patterns. These weak reflections are usually ignored. However, they provide an invaluable source of information on the atomic ordering which can be extracted by application of the (3+1)-dimension symmetry model. As a consequence, correlation between crystal structure and luminescence parameters can be much more precisely deciphered than in previous work. In this paper, we exemplify the potential of this concept with the
$Na_xEu_{3+(2-x)/3}MoO_4$ ($0 \le x \le 0.5$) series by solving the structure of six samples of different composition and relating their photo-physical parameters to the nature and amount of Eu aggregates present in the scheelites.

Powder diffraction data were collected on the Swiss-Norwegian Beam Line BM01A at the ESRF, Grenoble. $Na_{0.5}Eu_{0.5}MoO_4$ and $Na_{0.286}Eu_{0.571}MoO_4$ have been refined in the conventional I21/a space group with statistically distributed cations Na and Eu.

According to the scheme proposed for SRC, the I2/b(αβ0)00 (3 + 1)D superspace group has been applied here for all other incommensurately modulated structures and earlier for $Eu^{3+}_{2/3}MoO_4$. The magnified lower angle parts of powder diffraction patterns of the $Na_xEu^{3+}_{(2-x)}MoO_4$ compounds are shown in Fig.1. The luminescence properties of scheelite related compounds are essentially affected by the presence of Eu^{3+} aggregates, as shown from eight samples of the $Na_xEu^{3+}_{(2-x)/3}MoO_4$ series. Different amounts of Eu^{3+}-dimers have been detected in six modulated and ordered crystal structures, characterized by the weak satellite reflections appearing in the lower angle part of their XRD pattern. Two types of Eu-aggregates can be distinguished in the ordered structures: first, the Eu^{3+}-dimers or diatomic clusters (Fig.2) similar to those evidenced recently in silicate AV-24, and secondly, complex layers which are parallel to the *c* axis and normal to the modulation vector *q*. The shortest Eu–Eu distance is equal to about 3.95 Å in both types of Eu-aggregates, whereas the shortest Eu–Eu distance between aggregates is longer than 5.1Å. In the *ab* projection of a portion of cationic subsets (Fig.2), the Eu^{3+}-dimers can be recognized as Eu-pairs isolated from all other Eu-atoms by Na^+ cations and vacancies.

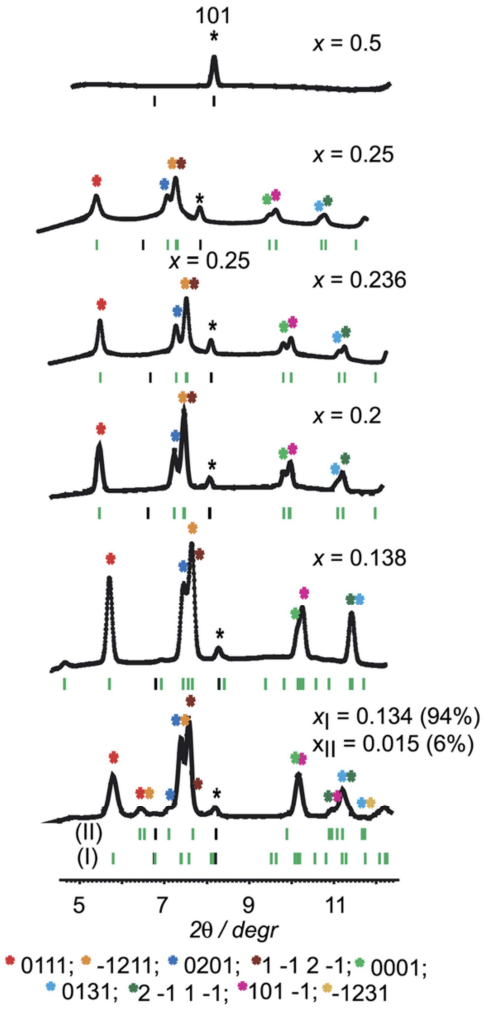

Figure 1. Magnified lower angle parts of the experimental XRD patterns of $Nax Eu_{3+(2-x)/3}MoO_4$ compounds with different compositions defined by *x*. Colored stars (corresponding to the nine different *hklm* indexes) and green strips indicate the satellite reflections.

This study points to the importance of considering the superspace formalism without which no direct correlation could be found between composition and luminescent properties of the material. Once the superspace model is established, it is straightforward to explore all the configuration modes and deduce the structures with the largest number of Eu^{3+} dimers in order to maximize luminescence. With this in mind, we can claim that the superspace concept represents a predictive tool for the discovery of new physical properties in material sciences.

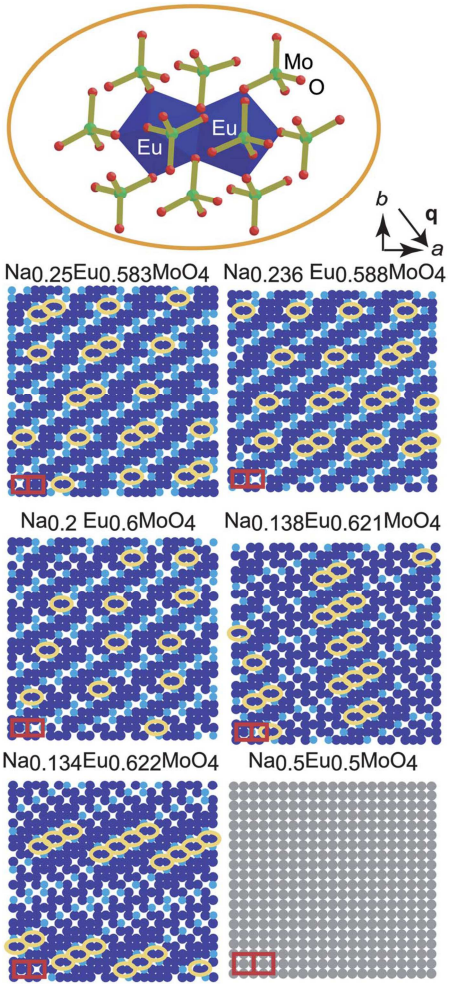

Figure 2. Portions of the *ab* projection of the cation subset in $Na_xEu^{3+}_{(2-x)/3}MoO_4$ compounds. Dark and light blue colors correspond to Eu and Na atoms, respectively, in the aperiodically ordered structures; grey indicates a mixture (Eu, Na) position in the disordered structure. Vacancies appear as large white stars. Eu dimers are surrounded by yellow contours. In the aperiodically ordered structures, the cation distribution differs in each adjacent unit cell (examples are indicated by red squares), whereas they are identical in the disordered one.

Principal publication:

Arakcheeva, A., Logvinovich, D., Chapuis, G., Morozov, V., Eliseeva, S., Bünzli, J.-C., Pattison, P. *Chem. Sci.,**3**, 384-390, 2012*

Fischer–Tropsch synthesis: An XAS/XRPD combined in situ study from catalyst activation to deactivation

Nikolaos E. Tsakoumis[a], Alexey Voronov[a], Magnus Rønning[a], Wouter van Beek[b], Øyvind Borg[c], Erling Rytter[a,c], Anders Holmen[a,*]

[a]Department of Chemical Engineering, Norwegian University of Science and Technology (NTNU), Trondheim, Norway.
[b]The Swiss-Norwegian Beam Lines (SNBL) at ESRF, BP 220, F-38043 Grenoble, France.
[c]Statoil R&D, Research Centre, Postuttak, NO-7005 Trondheim, Norway.

A Re promoted Co/γ-Al_2O_3 and an un-promoted Co/γ-Al_2O_3 Fischer–Tropsch catalysts were studied *in situ* throughout the common steps of laboratory catalyst testing i.e. reduction, pressurization, the initial period before reaching pseudo-steady state, deactivation and post mortem analysis. High-resolution X-ray powder diffraction (HR-XRPD) was combined with X-ray absorption spectroscopy (XAS) in order to reveal changes occurring during the experimental procedure. A mass spectrometer (MS) connected to the reactor outlet allow monitoring of the gas phase and accordingly the catalyst performance with respect to activity. Fischer–Tropsch synthesis was performed at industrially relevant conditions (493 K, 18 bar, H_2/CO=2.1 and >50% CO conversion).

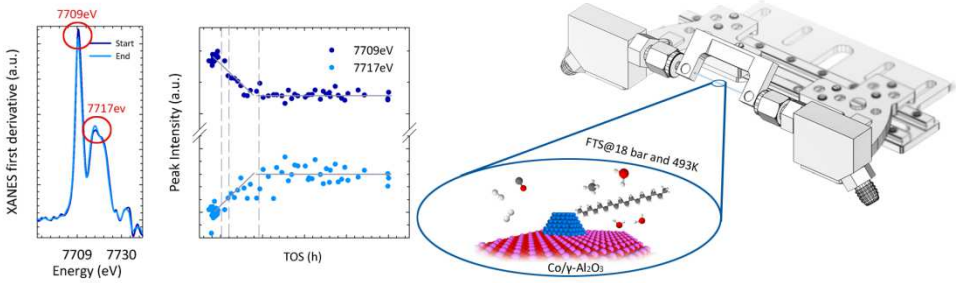

Motivation

Co-based catalysts appear more attractive for the conversion of natural gas derived synthesis gas to hydrocarbons, due to their high activity per pass, high selectivity to linear paraffin's, and low water–gas shift activity. However, because of the high price of the Co metal, catalyst stability has become a major issue to be addressed and a lot of effort has been devoted to deactivation studies from both industry and academia [1]. Ultimately, all supported FTS cobalt catalysts lose activity with time on stream. The main causes of catalyst deactivation as they are documented in the literature are poisoning, formation of inactive cobalt phases (re-oxidation, carbidization, and metal-support mixed compound formation), sintering, carbon formation, surface reconstruction, and attrition.

The investigation of the origin of catalyst deactivation in all catalytic applications is primarily a characterization-oriented subject, and commonly, the employed analytical procedures are applied *ex situ* on spent catalysts, *in situ* at moderate conditions or under vacuum on model systems [1–3]. *Ex situ* characterization of FTS cobalt catalysts requires a demanding sample handling since the results can be significantly affected by the pyrophoric nature of metallic Co existing in the spent catalyst. Furthermore, the procedure is hampered by catalyst encapsulation by long-chain hydrocarbons (FTS waxes). In addition, at reaction conditions the partial

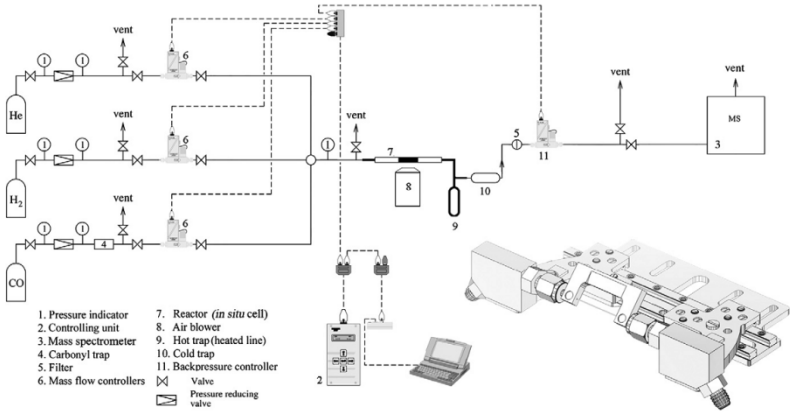

Figure 1. Sketch of the experimental setup and a 3D drawing of the in situ cell.

pressures of reactants and products dramatically affect catalyst behaviour. The impact of the gaseous FTS environment toward potential re-oxidation (high partial pressures of steam) or reconstruction during reaction makes the use of realistic FTS conditions vital. *In situ* and preferably *operando* studies of well-defined catalytic systems at realistic conditions have been employed by combining various complementary techniques in order to increase our understanding in the complicated Fischer–Tropsch synthesis reaction [1,2,4,5].

Catalyst activation

Data deriving from *in situ* XANES on the Co k edge (7709 eV) suggests that the reduction of calcined catalyst passes through a two-step procedure as previously reported[2]. The transition from Co_3O_4 via a CoO intermediate to metallic cobalt and a fraction of unreduced Co is illustrated by XANES (Fig. 2). A mixture of face centred cubic (*fcc)* Co and hexagonal close packed (*hcp)* Co on the reduced catalysts could be identified by XRPD. Full pattern decomposition by models of pure Co-*fcc* and Co-*hcp* crystallites was not viable indicating the intergrowth of the two phases and possible existence of staking faults or other grain boundaries[4].

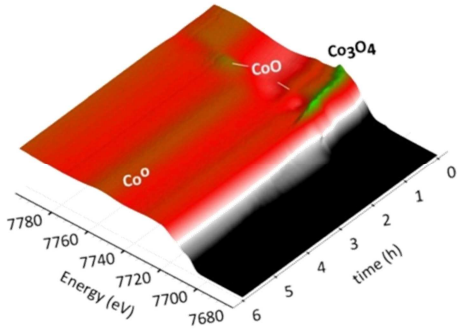

Figure 2. 3D representation of the species detected by Co-XANES during catalyst reduction at a ramp rate of 3°C/min to 400°C and dwell for 4 hours.

Quantitative results obtained by linear combination analysis of reference materials (cobalt oxides and foils) allowed evaluation of the reduction rates of Rhenium (Re)

promoted Co-Re/γ-Al_2O_3 and un-promoted Co/γ-Al_2O_3 catalysts. It appears that Re addition accelerated only the second reduction step from CoO to metallic cobalt.

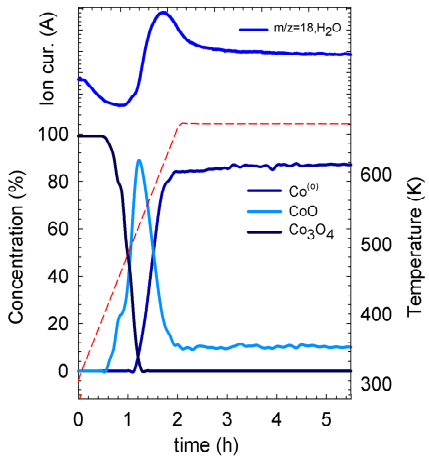

Figure 3. The formation of water as monitored by mass spectrometry together with the concentration of Co species during reduction.

Hydrocarbon synthesis

The reduced catalyst was subjected at realistic Fischer-Tropsch synthesis (FTS) environment for 40 hours. A quartz capillary reactor was used. Activity and deactivation behaviour shows good agreement with results obtained from a laboratory fixed-bed reactor (Fig. 4). Throughout the experiment a large number of X-ray scans were recorded showing very good repeatability and allowing detection of minor changes. Pressurization, induction period and steady-state/deactivation period were studied. Different observations in each of them are briefly discussed.

Already at the pressurization under synthesis gas environment it is expected that the cobalt surface reconstructs due to the invasive nature of CO. However, no change in the EXAFS signal was detected during that period. Here it should be mentioned that the surface to volume ratio of cobalt particles in the present study (0.085) may be insufficient for such information to be extracted.

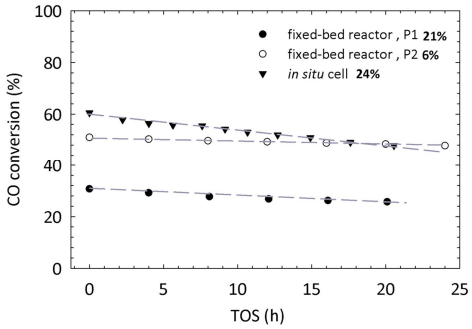

Figure 4. FTS activity profile from FBR and the in situ cell.

During the induction period XANES data suggest re-oxidation of the Re-promoted catalyst into a divalent cobalt (Co^{+2}) in the expense of metallic Co. Apparently a reduction in the feature related to metallic cobalt at edge energy is more observable than the formation of the divalent cobalt phase (Fig. 5).

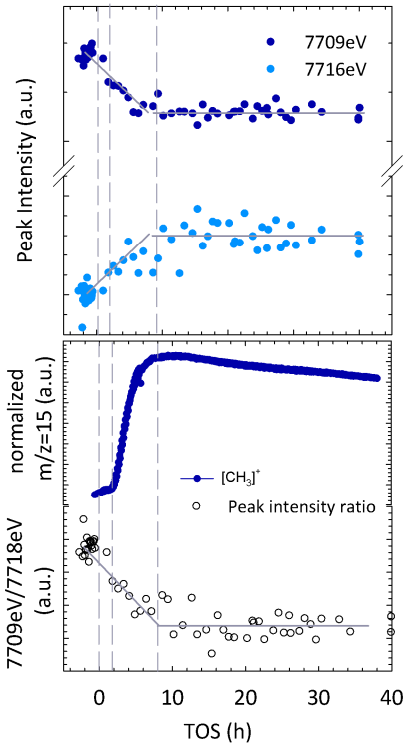

Figure 5. Evolution of features existing in the first derivative of XANES spectra and related to metallic and Co^{+2} phases (upper) MS signal of the methane formation (lower).

Simulation by linearly combined XANES spectra of the clearly demonstrated that the formed species are closer to the tetrahedral configuration found in the surface $CoAl_2O_4$–like compound or wurtzite-type CoO than the octahedrally coordinated CoO. Water may play a key role in this transformation since it is been produced throughout the induction period and is known to interact with the alumina surface by a hydrating mechanism and Co.

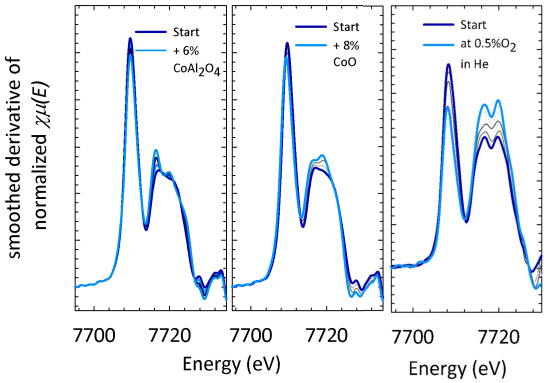

Figure 6. Simulation of the formation of $CoAl_2O_4$, CoO on reduced catalyst Co-Re/γ-Al_2O_3 catalyst together with model experiments on reduced catalyst under diluted O_2 stream.

This result implies that a mechanism of aluminate formation passes directly from the metallic cobalt to the Co-aluminate compound, without the CoO intermediate. However, the resolution of the technique in addition to the broad size distribution of the high surface area catalyst may be insufficient to detect such an intermediate. Alternatively, the formation of a wurtzite-type CoO at FTS conditions should not be

excluded. On the other hand the Co/γ-Al_2O_3 catalyst exhibits further reduction during the evolution of reaction as was previously shown [2].

From the correlation of the MS signal and the XANES spectra it is evident that the formation of divalent cobalt is taking place during the induction period and not in the steady-state Fischer-Tropsch synthesis. In addition, it is encountered only in the promoted catalyst. Similar results have been obtained by temperature programmed and gravimetric techniques or ex situ XANES on spent catalysts by other researchers. Though, the interpretation was different since the ex situ studies lack a clear overview of the reaction evolution with time. Work from our group [6] on the effect of water in similar catalysts is suggesting a rapid irreversible deactivation of the small Co particles when high partial pressures of steam are introduced.

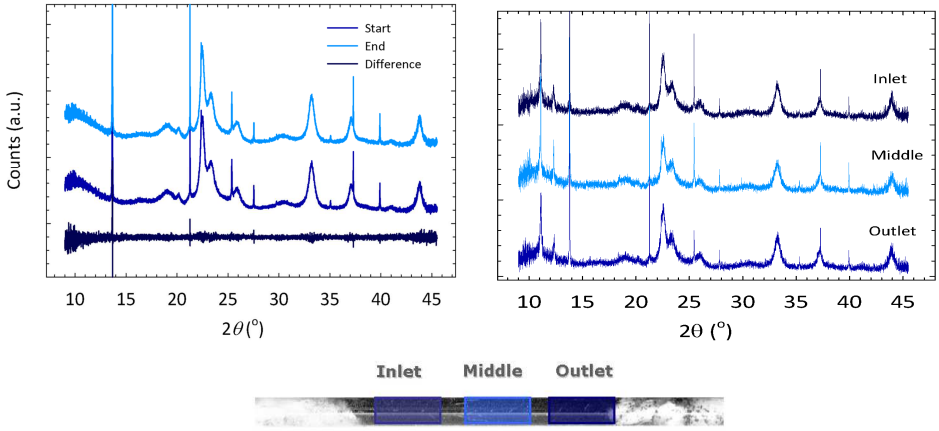

Figure 7. XRPD patterns of the catalyst after reduction and after 40h of FTS (upper). The different parts of the catalytic bed were probed (lower).

Monitoring of the catalyst during the Fischer – Tropsch synthesis at industrially relevant conditions by using a combination of X-ray characterization techniques with simultaneous activity measurements, suggests that the bulk of the cobalt remains unaffected during the run. That implies absence of bulk transformations that previously have been proposed to be reasons for the initial deactivation in FTS (i.e. re-oxidation and carbide formation). No indication of crystallite growth due to sintering was detected during the run (Fig. 7). In addition no significant gradients in the concentration of cobalt species or the size of the crystallites has been found as a function of the length of the catalytic bed (Fig. 7 and 8).

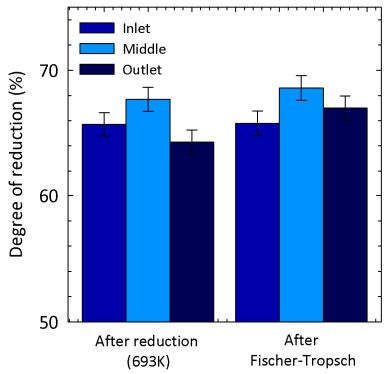

Figure 8. Degree of reduction as a function of catalyst bed position before and after FTS.

Summary

Common laboratory FTS activity test has been performed into a micro-system using a quartz capillary as reactor. Two catalysts were tested: Co-Re/γ-Al_2O_3 and a Co/γ-Al_2O_3. The setup has been optimized for performing FTS for more than a day at industrially relevant conditions (18 bar, 493 K, and CO conversion >50%). XAS and HR-XRPD were combined in order to reveal information on the catalyst phases during all the stages of the experimental procedure. The induction period appears to be of particular interest since the formation of tetrahedrally coordinated divalent cobalt is detected in the Co-Re/γ-Al_2O_3 catalyst. The phase appears to be similar to a surface $CoAl_2O_4$-like compound. On contrary the Co/γ-Al_2O_3 catalyst is subjected to further reduction during the induction and reaction periods. This further reduction is mainly taking place at the outlet of the reactor. Initial deactivation was detected by the MS but no apparent change in the X-ray signal could be observed. Results suggest that catalyst deactivation observed in the inisiat stages of FTS is surface-related phenomenon.

Acknowledgements

This publication forms a part of the inGAP (Innovative Natural Gas Processes and Products) Centre of Research-based Innovation, which receives financial support from the Norwegian Research Council under Contract No. 174893. The authors would like to thank the Norwegian Research Council and Statoil for financial support through the inGAP project

Publications

[1] N. E. Tsakoumis, M. Rønning, Ø. Borg, E. Rytter, A. Holmen, *Catalysis Today* **2010**, *154*, 162–182.
[2] M. Rønning, N. E. Tsakoumis, A. Voronov, R. E. Johnsen, P. Norby, W. van Beek, Ø. Borg, E. Rytter, A. Holmen, *Catalysis Today* **2010**, *155*, 289–295.
[3] N. E. Tsakoumis, Deactivation of Cobalt-based Fischer-Tropsch Synthesis Catalysts, **2011**.
[4] N. E. Tsakoumis, R. Dehghan, R. E. Johnsen, A. Voronov, W. van Beek, J. C. Walmsley, Ø. Borg, E. Rytter, D. Chen, M. Rønning, et al., *Catalysis Today* **2012**, 10.1016/j.cattod.2012.08.041.
[5] N. E. Tsakoumis, A. Voronov, M. Rønning, W. van Beek, Ø. Borg, E. Rytter, A. Holmen, *Journal of Catalysis* **2012**, *291*, 138–148.
[6]S. Lögdberg, M. Boutonnet, J. C. Walmsley, S. Järås, A. Holmen, E. A. Blekkan, *Applied Catalysis A: General* **2011**, *393*, 109–121.

Porous and Dense Magnesium Borohydride Frameworks: Synthesis, Stability, and Reversible Absorption of Guest Species

Y. Filinchuk[a,b,c], B. Richter[b], T.R. Jensen[b], V. Dmitriev[c], D. Chernyshov[c], H. Hagemann[d]

(a) Université Catholique de Louvain (Belgium); (b) Aarhus University (Denmark)
(c) SNBL at ESRF (France); (d) University of Geneva (Switzerland)

Crystalline hydrides, made of hydrogen and light elements such as boron, contain huge quantities of hydrogen but do not release it easily, due to their strong chemical bonds. Scientists have now, for the first time, succeeded in crystallising a highly porous hydride that can take up even more gas and release this additional amount when needed, like a reservoir or a gas bottle. The results are published in Angewandte Chemie, and highlighted by an inside cover page in the November 2011 issue.

The international team included researchers from the universities of Louvain-la-Neuve (Belgium), Aarhus (Denmark) and Geneva (Switzerland), along with the European Synchrotron Radiation Facility. The main author is Yaroslav Filinchuk from the Université Catholique de Louvain, University of Aarhus and ESRF.

Hydrogen is the most promising candidate fuel for future clean cars and trucks. The main reason it is not widely used today is the lack of affordable and safe mobile storage systems. Research into storage systems is focusing on two classes of materials: complex hydrides containing light elements such as boron, nitrogen or aluminium (borohydrides, amides, alanates); and porous materials, so-called metal-organic frameworks (MOFs). Unfortunately, whilst hydrides store large amounts of hydrogen, they release it only at relatively high temperatures. On the other hand, MOFs store and release molecular hydrogen easily, but only at cryogenic temperatures. The two groups of materials are made of completely different building blocks, representing two diverse fields of chemistry.

The new substance, obtained by Bo Richter from the University of Aarhus, combines the properties of both: it is highly porous like a MOF but entirely made of a hydride. This new form of magnesium borohydride (γ-$Mg(BH_4)_2$) stores 15 weight percent of hydrogen in the bulk material, representing an energy density equivalent to 50% of that of diesel fuel. In the pores, the material has the capability to store another 3 weight percents of H_2, at low temperatures, which alone represent 5 times the energy density of a modern lithium-ion battery.

As the material is crystalline, the researchers could study its gas uptake and release as well as its pressure- and temperature-induced transformations by X-ray diffraction. Most of these experiments were carried out at BM01A. The scientists discovered that about one third of the new material is empty and this space can store various guest molecules, including hydrogen, nitrogen and even small organic molecules. It holds these gases at higher temperatures than most other porous solids. The nature of

interaction between the "guest" gas molecules and the "host" nanoporous framework was also revealed by X-ray diffraction.

Information on the structure and properties of the new material allowed the researchers to infer the nature of the chemical bonds and building principles in metal borohydrides. This research opens a door, via combining the BH_4 anions with more complex ligands, to novel hybrid materials which could be highly selective gas storage and/or separation systems.

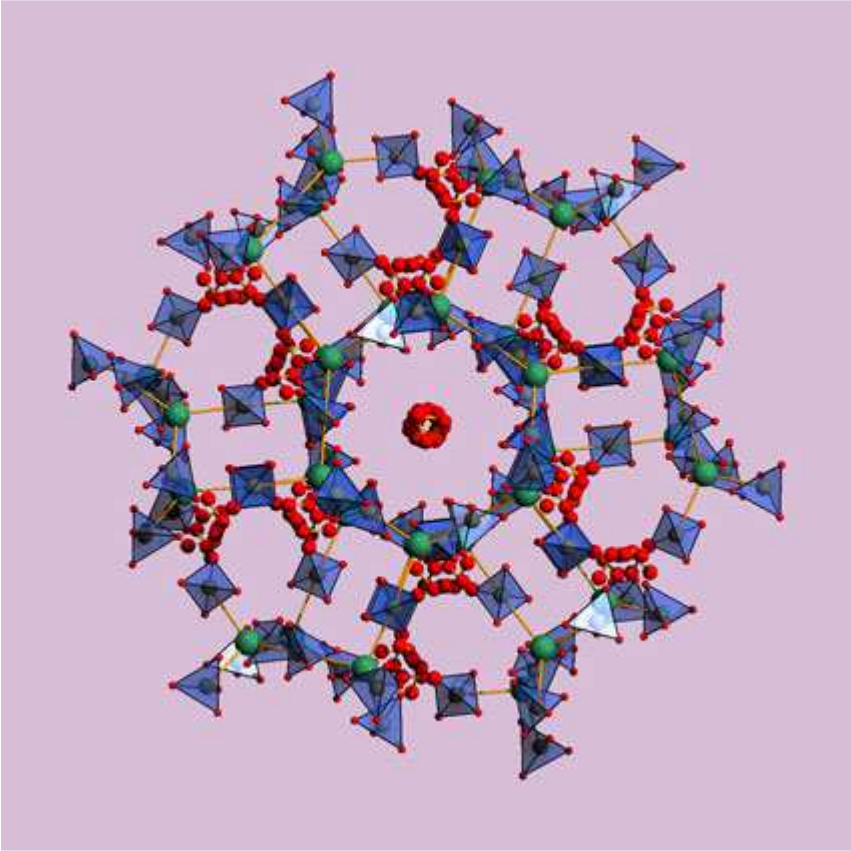

Hydrogen gas molecules (red spheres) stored within the crystalline magnesium borohydride structure (Mg green, BH_4 blue).

Publication

Y. Filinchuk, B. Richter, T.R. Jensen, V. Dmitriev, D. Chernyshov, H. Hagemann, Porous and Dense Magnesium Borohydride Frameworks: Synthesis, Stability, and Reversible Absorption of Guest Species, *Angew. Chem. Int. Ed.* **50**, 47, 11162–11166, 2011

Crystal structure determination of the first borohydrides borate, $Ca_3(BH_4)_3(BO_3)$

M. D. Riktor[1], Y. Filinchuk[2], M. H. Sørby[1]and B. C. Hauback[1]

[1]Physics Department, Institute for Energy Technology, P. O. Box 40, NO-2027 Kjeller, Norway
[2]Swiss-Norwegian Beam Lines at ESRF, BP-220, 38043 Grenoble, France

Effective storage of hydrogen is a major bottleneck for implementation of a hydrogen-based energy economy. Metal hydrides offer a safe and very compact way to store hydrogen, however the weight of metal hydrides based on transition metals is impractically high for vehicular applications. After the discovery of reversible hydrogen desorption from Ti-catalyzed $NaAlH_4$ [1], a lot of attention has been devoted to complex hydrides based on aluminum and boron. Many borohydrides have superb hydrogen capacities, e.g. 18.5 wt%H in $LiBH_4$, 14.9 wt%H in $Mg(BH_4)_2$ and 11.6 wt%H in $Ca(BH_4)_2$. These are hampered by high desorption temperatures of hydrogen. However, theoretical calculations conclude that $Mg(BH_4)_2$ and $Ca(BH_4)_2$ should desorb hydrogen around 100 ^oC [2, 3] which is ideal for coupling with PEM fuel cells. This indicates that the high decomposition temperatures that are observed experimentally could be due to kinetic rather than thermodynamic limitations. Moreover, $Ca(BH_4)_2$ has shown some promise regarding reversibility at feasible conditions [4, 5].

Experimental studies of $Ca(BH_4)_2$ has revealed an unusually complicated crystal chemistry. Four polymorphs, α-,α'-, β- and γ-$Ca(BH_4)_2$ has been identified and structurally characterized. A previous in-situ powder diffraction investigation at SNBL reported that γ-$Ca(BH_4)_2$ rapidly transformed into a new phase around 300^oC without significant gas release [6]. It was therefore assumed that the new phase was a fifth modification of $Ca(BH_4)_2$, denoted "δ-$Ca(BH_4)_2$". Due to the small amount of this "δ"-phase in the sample and the limit resolution of the in-situ data, the structure of the new phase was not solved.

From the observations that the "δ"-phase is formed less readily from the high-temperature β-modifications than α- and γ-$Ca(BH_4)_2$ [6, 7], synthesis of a purer "δ"-phase sample was attempted by a cyclic approach. A sample consisting of mostly α- and γ-$Ca(^{11}BD_4)_2$ was heated to 340 ^oC which is above the previously observed temperature of formation for the "δ"-phase but below the decomposition temperature[1]. The sample was then annealed at 165 ^oC for 96 hours to revert some of the β-$Ca(BH_4)_2$ which is formed above ~ 180^oC, back to the low-temperature modifications α- $Ca(BH_4)_2$ before heating again to 340^oC. After three such cycles, the sample contained the "δ"-phase as the only crystalline constituent, as shown in the high-resolution SR powder diffraction data (BM01B) in Figure 1. The three-times-cycled sample was also measured at with the MAR345 image plate at BM01A.

The high-resolution data were used for indexing (a = 8.995 Å, b = 8.052 Å c = 11.767 Å) while structure solution was carried out with the FOX software [8] using the image plate data due to the superior counting statistics and simpler profile shapes. No structure solution could be found under the assumption that the phase was a calcium

[1] The isotopes ^{11}B and D (^2H) where used rather than natural boron and hydrogen to facilitate neutron diffraction experiments. However, the amount of synthesized materials was too small to neutron diffraction. The isotopic notation is omitted in the rest of the text for simplicity.

borohydrides. When variable occupancy was allowed for the lighter atoms, some refined to values higher than 1 thus indicating the presence of stronger scatterers. These were identified as oxygen atoms and the structure could be solved with a mixture of tetrahedral borohydrides (BH_4^-) and triangular borate (BO_3^{3-}) anions giving the composition was $Ca_3(BH_4)_3(BO_3)$ [9]. A search in ICSD revealed no compounds with both B-H and B-O bonds, thus showing that this is an entirely new class of compound. The structure was refined with the Rietveld method using the high-resolution- and image plate data simultaneously. The obtained fits are shown in Figure 2 and the refined structure model is shown in Figure 3.

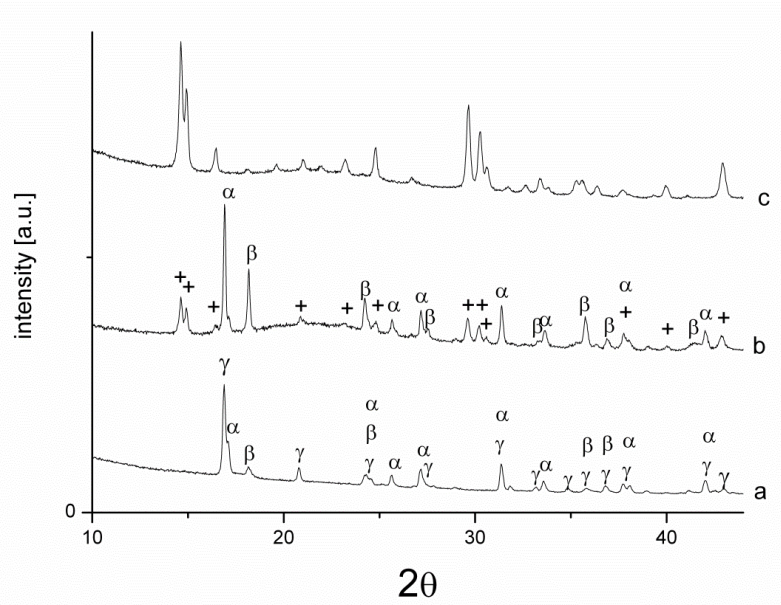

Figure 1. High-resolution SR powder diffraction data (BM01B) for a) as-syntesized $Ca(BH_4)_2$, b) sample after one heating cycle and c) sample after 3 heating cycles. + indicate Bragg peaks from $Ca_3(BH_4)_3(BO_3)$, formally known as "δ"-phase. Greek letters indicate different modifications of $Ca(BH_4)_2$

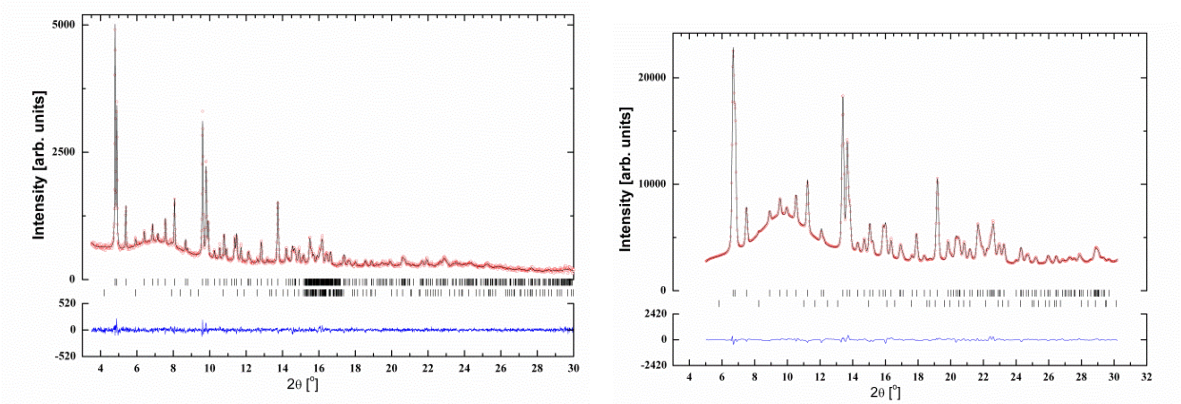

Figure 2. Rietveld fit to high-resolution (BM01B, left) and image plate (BM01A, right) SR powder diffraction data for $Ca_3(BH_4)_3(BO_3)$. The top row of tick marks indicate the Bragg peak position for the borohydrides borate. The lower tick marks indicate peaks from a minor amount of β-$Ca(BH_4)_2$.

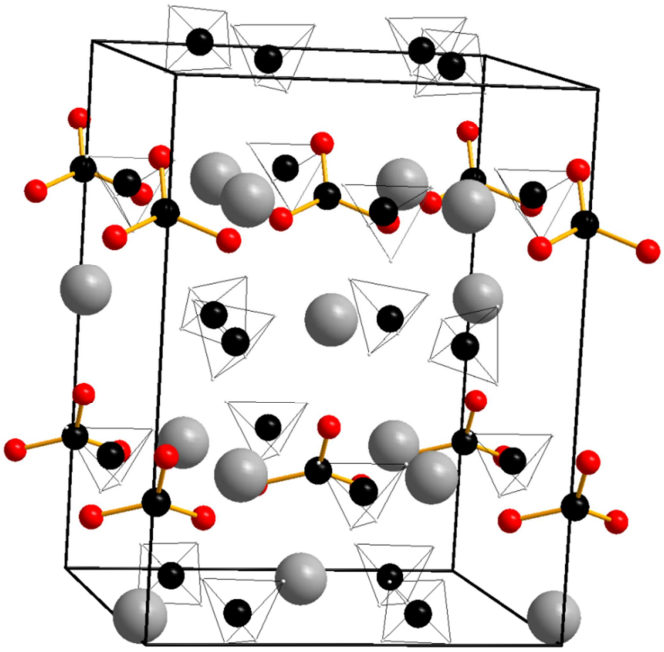

Figure 3 Refined structure model of $Ca_3(BH_4)(BO_3)$

$Ca_3(BH_4)_3(BO_3)$ have two crystallographically different Ca^{2+} cations which are both coordinated by four BH_4^- and two BO_3^{3-} anions in a strongly distorted octahedral coordination. It is interesting to note that all known polymorphs of $Ca(BH_4)_2$ also have distorted octahedral coordinations of anions around the cation, although the degrees of distortion are less than in $Ca_3(BH_4)_3(BO_3)$.
The source of the oxygen needed to form the borohydride borate is not known. However, it seems implausible that enough oxygen could leak from the atmosphere to the sample during the cycling. Thus, it is likely that the oxygen was present in the starting material in an X-ray amorphous state, possibly as boric acid (H_3BO_3). The report of formation of this novel boride-containing phase from seemingly pure $Ca(BH_4)_2$ has increased the awareness in the hydrogen storage community of the importance of thorough quality check of starting materials, also with non-diffraction techniques to reveal amorphous impurities. Moreover, it may shed new light on the mechanisms for oxidation of borohydrides.

References

[1] B. Bogdanovic, M. Schwickardi, Ti-doped alkali metal aluminium hydrides as potential novel reversible hydrogen storage materials, *J. Alloys Comp*., **253-254** (1997) 1-9.
[2] K. Miwa, M. Aoki, T. Noritake, N. Ohba, Y. Nakamori, S. Towata, A. Zuttel, S. Orimo, Thermodynamical stability of calcium borohydride $Ca(BH_4)_2$, *Phys. Rev. B*, **74** (2006) 155122.
[3] Y. Nakamori, K. Miwa, A. Ninomiya, H.W. Li, N. Ohba, S.I. Towata, A. Zuttel, S.I. Orimo, Correlation between thermodynamical stabilities of metal borohydrides and cation electronegativites: First-principles calculations and experiments, *Phys. Rev. B*, **74** (2006) 045126.

[4] J.-H. Kim, J.-H. Shim, Y.W. Cho, On the reversibility of hydrogen storage in Ti- and Nb-catalyzed $Ca(BH_4)_2$, *Journal of Power Sources*, **181** (2008) 140-143.
[5] E. Rønnebro, E.H. Majzoub, Calcium borohydride for hydrogen storage: Catalysis and reversibility, *J. Phys. Chem. B*, **111** (2007) 12045-12047.
[6] M.D. Riktor, M.H. Sørby, K. Chlopek, M. Fichtner, F. Buchter, A. Zuettel, B.C. Hauback, In situ synchrotron diffraction studies of phase transitions and thermal decomposition of $Mg(BH_4)_2$ and $Ca(BH_4)_2$, *Journal of Materials Chemistry*, **17** (2007) 4939-4942.
[7] A. Nickels, W.I.F. David, in: *Symposium on Metal-Hydrogen Systems*, Reykjavik, Iceland, 2008.
[8] V. Favre-Nicolin, R. Cerny, A better FOX: using flexible modelling and maximum likelihood to improve diect-space ab initio structure determination from powder diffraction, *Zeitschrift fûr Kristallographie*, **219** (2004) 847-856.
[9] M.D. Riktor, Y. Filinchuk, P. Vajeeston, E.G. Bardaji, M. Fichtner, H. Fjellvag, M.H. Sorby, B.C. Hauback, The crystal structure of the first borohydride borate, $Ca_3(BD_4)_3(BO_3)$, *Journal of Materials Chemistry*, **21** (2011) 7188-7193.

STATUS OF FACILITY

BM01A

We have been able to maintain the high productivity of the beamline during the years 2011-2012, with about 60 publications per annum coming from data collected at BM01A. Despite the closure of the entire facility for several months early in 2012 (as part of the upgrade of the ESRF), there has been little or no impact on the output from the beamline. It was possible, however, to take advantage of the enforced shut-down in order to make some major improvements to the equipment on the experimental station. The main efforts and resources on BM01A have been concerned with upgrading the X-ray area detectors used on the beamline, and we will describe the impact of these developments in the following sections in more detail.

The range of activities on BM01A has continued to be very wide, including both powder and single crystal experiments and cover scientific topics from chemical crystallography to the physical sciences. The main theme has continued to be the investigation of structure-property relationships. Particularly challenging is the borderline region between ordered and disordered structures, where both Bragg and diffuse scattering may play a role. Our new detectors have opened up many interesting possibilities in this domain, and it is likely to become more and more important in the coming years. The excellent detector performance has also allowed the time resolution of the diffraction experiments to be shortened dramatically. These improvements, together with the better data quality delivered by our detectors, have encouraged our user community to explore new possibilities for in-situ experiments. Although powder diffraction is the main technique for following chemical reactions, the speed of data collection is now so rapid that even single crystals can be investigated on the time-scale of a few minutes per data set. The intensity available even on a bending magnet is more than sufficient to allow high quality data to be collected in a remarkably short time for most samples. Until recently, time constraints meant that only a few single crystal data sets were collected per project. Now it is perfectly possible to collect hundreds of data sets per day. This, in turn, allows detailed systematic studies of the response of crystals to changes in, for example, temperature, pressure or chemical environment to be carried out within a reasonable timescale.

The collaborations between the beamline staff and various other groups and facilities continue to be very fruitful. The experiments carried out jointly by members of the PSI Laboratory of Neutron Scattering and SNBL have led to several publications over the past two years, principally in the fields of new superconductors and relaxor ferroelectrics. The work on interpreting diffuse X-ray scattering together with the inelastic scattering group of the ESRF has also led to some excellent papers. On a more formal level, we continue our exchange of beamtime and resources with the Dutch-Belgian beamline, to the mutual benefit of both groups. In addition, the collaboration agreement with Maxlab begins to bear fruit, and the upgrade of the controls of our KM6 diffractometer will be done together with the controls group of Maxlab (who operate a similar instrument equipped with an identical CCD detector). More details of these developments will be given below.

KM6CCD diffractometer

The Committee of the Future of SNBL concluded in 2008 that the most important developments foreseen for BM01A concerned the replacement of the aging detectors. In the case of the KUMA diffractometer, the Onyx CCD from Oxford Diffraction Ltd has been in continuous and successful operation for almost a decade, and has produced many thousands of data sets and a large number of publications. However, the Committee highlighted the need to replace the CCD detector with one of the latest generation, with improvements in dynamic range and faster read-out time. Using internal funding through the SNX budget, a Titan CCD could be purchased from Agilent and installed on the KM6 diffractometer in 2011.

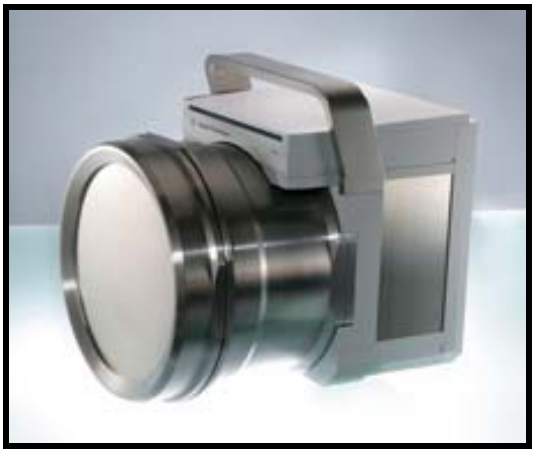

Fig 1. The new Titan CCD installed on the KM6 diffractometer

The installation was made on 24 March, and the first users could profit from access to the new detector already on 6 April 2011. In addition to the recommendation to replace the CCD, the Committee also strongly encouraged the SNBL team to change the diffractometer software controls to the ESRF standard (called SPEC). In the summer of 2012, the industrial computer running the KM6 control software failed, and a repair of the obsolete hardware was no longer possible. It was therefore time to follow the recommendations of the Committee, and work on this controls project is now in progress. Since a beamline at Maxlab operates an identical detector on a diffractometer constructed by Newport Ltd, was have agreed to collaborate with Maxlab on the development and commissioning of a common software platform for diffractometer controls.

Pilatus2M upgrade

With the aid of generous funding from Switzerland and Norway, it was possible to place an order in 2011for the latest generation of large area pixel detectors produced by Dectris Ltd (Baden). In addition to the Pilatus2M detector itself, the funds were sufficient to cover the costs of a new and versatile platform and kappa goniometry suitable for a wide range of different experiments in diffraction and X-ray scattering. The complete instrumentation was delivered and installed during the shut-down of the ESRF in the spring of 2012. The first experiments with the new setup could be conducted in June, and the Pilatus2M has been in continuous use since its installation on BM01A. A comparison of the performance parameters compared with the image plate detector previously in use on BM01A underlines the dramatic improvements which the Pilatus2M

has brought to SNBL. Instead of about 1 minute read-out time for the image plate, the new detector can be read-out in 2ms. This reduction in cycle time allows a data collection to be made in shutter-less mode, which in turn speeds up the entire data collection procedure. A typical measurement time for a good quality single crystal data set has been reduced from 2 – 3 hours down to less than 10 minutes. This changes not only the quantity of measurements which can be carried out (and hence improves the through-put of the beamline), but changes also qualitatively the overall performance of the instrument. Fast experiments can mean also more reliable measurements, since they place less demands on the long-term stability of the beam itself and of the sample environment. It is also easy to repeat measurements in order to check the reproducibility of an experimental result. In addition, of course, fast experiments imply that we can more easily follow fast processes such as phase transitions, chemical reactions etc.
The Pilatus2M setup on BM01A has now been in operation for many months, and a very large number of data sets have been delivered to the users. The huge quantity of data which this implies brings its own challenges in terms of handling, processing and storing the images. Exactly this question of optimal data treatment and presentation is becoming more and more important, and several collaborations have begun with specific user groups interested in addressing this problem. In particular, groups from Stavanger and Trondheim wish to send scientists to SNBL for extended periods both to learn the how best to profit from the new instrumentation, and to optimize the data treatment.

Fig. 2. The new general-purpose platform for X-ray diffraction and scattering on BM01A

In addition to the data analysis, it is import to learn how best to design an optimal strategy for collecting the data. Fast data collection does not automatically imply that the data will be good, and we have established a close collaboration with Dectris Ltd in order to look carefully at data quality. This collaboration includes carrying out joint experiments at SNBL to investigate the factors which can have a negative impact on data quality, such as counter dead-time and saturation effects. The Pilatus2M detector on BM01A is probably the only instrument of this type already operational on a general-purpose beamline for X-ray diffraction and scattering experiments. This presents both challenges and opportunities both for our users and for the staff of SNBL in the coming months.

BM01B

SNBL is now looking back on almost 20 years of successful operation, and both stations (SNA as well as SNB) have undergone radical changes and improvements over the last years.
In the case of SNB the initial set-up of a basic Powder Diffraction (PD) and EXAFS station has long been surpassed with the specialization of the beamline towards the *in-situ* characterization of dynamically evolving systems, namely: catalysis, diffusion and intercalation processes, *in-situ* synthesis, phase transitions and many others. In the last report we have shown that SNB is now equipped with two sequential monochromators which can be interchanged within seconds. This allows for an almost instant swap between PD and EXAFS and thus the possibility to follow complex “real world” systems *in-operando* using both techniques. We are now in a situation where we can look at local ordering at a scale of typically ≈ 1nm using EXAFS together with PD covering the structural investigations of systems ≥ 100nm and – as described in previous reports – we do have the possibility of parallel use of Raman techniques covering (at least partly) the range between the two extremes. This set-up has been highly appreciated not only by our Swiss-Norwegian groups, but also by ESRF users where we regularly face a more than 10-fold oversubscription in terms of beam time requests on SNB. The high scientific output (seeSec.) can be used as a measure for the success of the station.
Despite the constant progress made over the last decade we think that we recently made another major leap forward. The progress made is essentially about the speed at which we can perform these combined measurements and will be outlined over the next pages.

Improvements on the EXAFS scheme

Since we have put our two crystal monochromator in operation in 2005, the data quality has improved considerably since. We have now added a fast scanning feature to this monochromator which brings the measurement time from typically 20-30 mins down to timescales below 20 or even 10 seconds, especially at energies ≤10keV where big angular changes slowed down the measurement speed in the past.

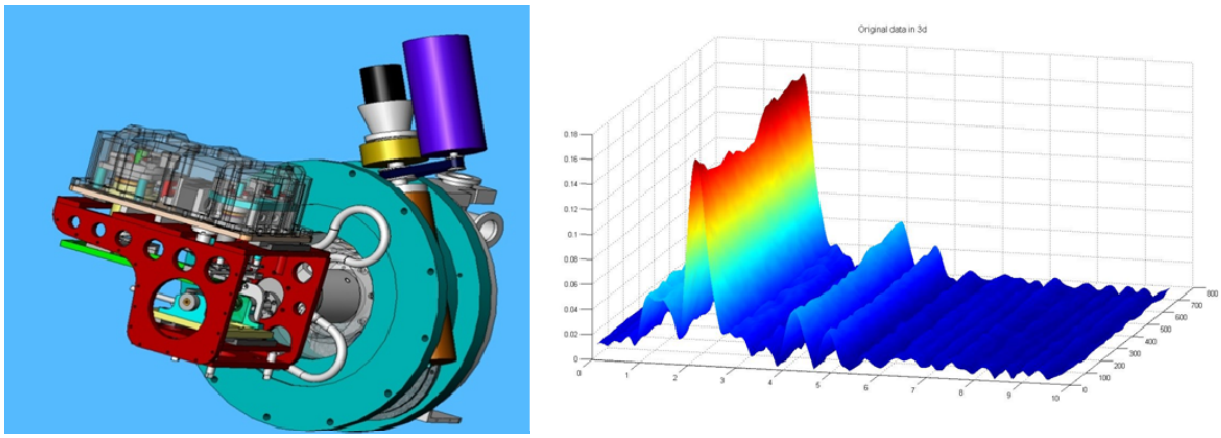

Figure 1. Left: XAFS monochromator with new fast scanning motor (violet), an electric clutch (yellow) and the old motor/gearbox system (black/gray), Right: typical carpet-like sequential measurements performed with the new fast scanning option

This feature has become particularly popular amongst the groups using modulation techniques (as presented in the last report) where sometimes hundreds of scans are performed on samples exposed to periodically changing outer stimuli, like variations in pressure, temperature or gas composition.
The improvements on the EXAFS side have however lead to a complete mismatch of the timescales needed for EXAFS and PD scans respectively.

Improvements on the Powder Diffractions scheme

A classical High Resolution Powder Diffraction measurement (HRPD) using our diffractometer can be performed on a time scale of typically ≥ 30min, thus far slower than the 20secs now needed for a full EXAFS scan. To overcome this mismatch we have recently acquired a 12 Megapixel, 2D medical detector (Dexela/Perking Elmer systems) which we commissioned for powder diffraction over the last weeks. This new system allows for stroboscopic measurements on the sub-second scale (possible read-out speed of ≈ 30 frames/sec) re-balancing the time needed for EXAFS and PD measurements.

Although the resolution of this system is lower than the HRPD option most industrially relevant systems do not need this very high resolution. Furthermore, looking at the new beam line scheme as shown below one realizes that the new 2D detector has been mounted below the plane defined by the X-ray beam.

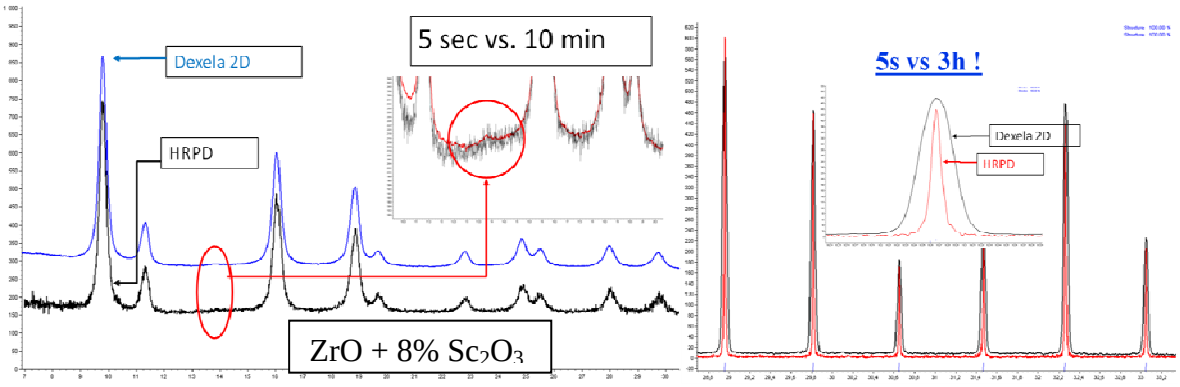

Figure 2. Comparison between the HRPD and the new Dexela 2D detector. Even small features (see red circles, left) are still well above the noise level despite the 5s exposition time for the 2D detector compared to the 10min for the HRPD ! The resolution is however 3 times lower (see right image).

We do now have the possibility to follow the reaction in HRPD in parallel with the new 2D-detector. We do so by recording the overall powder pattern using the 2D detector below the horizontal plane and following individual peaks (peak-width and possible splitting) with the HRPD. Furthermore the parallel use of the HRPD allows for a precise calibration of our powder patterns obtained with the 2D-detector.

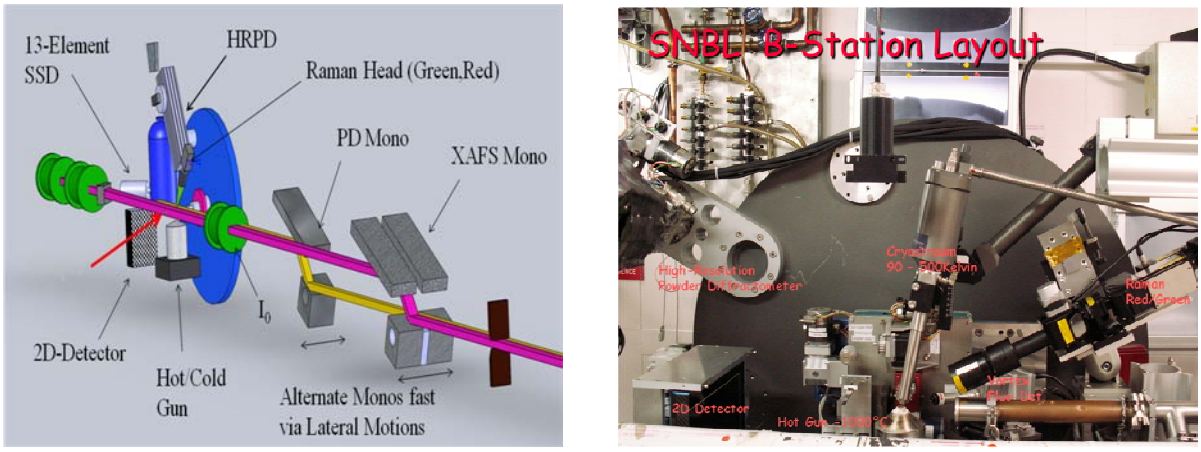

Figure 3. New beamline layout including the 2D detector

Changes in the Beamline Layout Scheme

The addition of new equipment and the ever increasing complexity of experiments made a complete refurbishment of the station layout necessary. The whole experimental set-up is now mounted on one central supporting marble block on which a series of X-95 profiles have been attached. They act like optical benches where we can arrange the position of samples, detectors, x-ray-eyes and flight tubes within minutes thus reducing the overhead we need to set up the beamline.

Outlook:

Total Scattering

The acquisition of the 2D detector has improved the performance of the beamline with respect to fast PD measurements enormously. There is however an additional side to it: In the introduction we defined the scales covered by EXAFS and PD (1nm vs. 100nm). Despite the Raman, the range in-between is still badly covered and we are now concentrating our efforts in adapting this new detector to Total Scattering or **P**air **D**istribution **F**unction (**PDF**) techniques, which could potentially close this gap. PDF requires a highly stable and reproducible detection scheme. Guided by a whole series of ideas we have, we are now in close contact with the producing company (Dexela) the software group t in order to reach this goal.

Moving SNB to a new Beamline Port

The pace at which progress has been made over the last couple of years becomes increasingly difficult to maintain due to the fact that the vicinity of the A-line crossing the Optics enclosure as well as in the B-station itself stymies our efforts to put additional (optical) components in. The improvements we aim at are namely the installation of a *pre-mono collimating mirror system* in order to gather more flux without degrading the resolution and to reduce the heat load/radiation damage on the downstream components. Secondly the implementation of a *post-mono deviating (and possibly focussing) mirrors system* which would allow to cross the x-ray beam used for PD on the same sample spot as the one used for EXAFS. This would allow to perform truly simultaneous PD/ EXAFS measurements as compared to the quasi-simultaneous/sequential measurements which we perform at present. Last not least: moving SNB to another beamline would allow us *to install a third monochromator* for high throughput as needed for PDF measurements.
To achieve these goals we handed in a proposal to the ESRF with the backing of the SNX last year. The ESRF has signalled that they are positive about our request and we hope that this move can be achieved in a foreseeable future

SNBL - FACTS AND FIGURES

BUDGET (in kCHF)

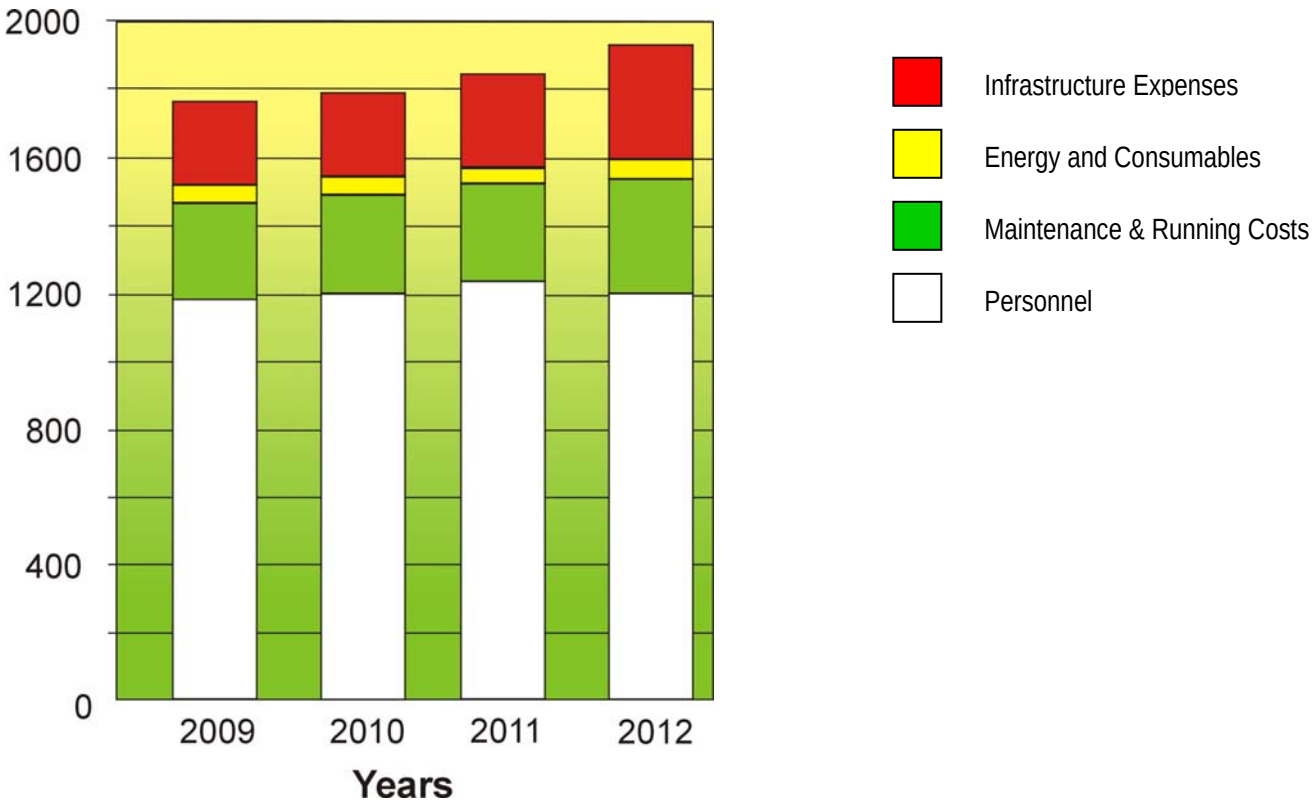

BUDGET in kCHF	2009	2010	2011	2012
Personnel	1,174	1,200	1,230	1,207
Maintenance and Running Costs	280	290	300	339
Energy and Consumables	52	53	55	60
Infrastructure Expenses	244	247	250	283
TOTAL	**1,750**	**1,790**	**1,835**	**1,889**

INCOME (in kCHF)

Income Outside Contract

Income According to Contract

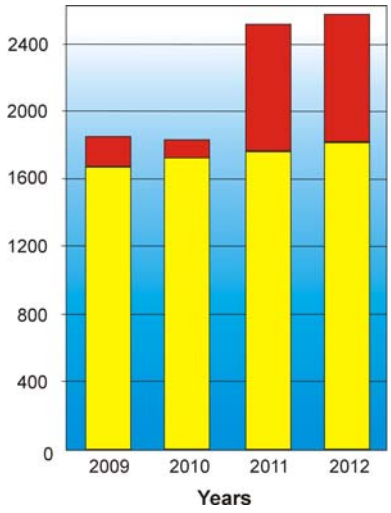

INCOME in kCHF	2009	2010	2011	2012
Income According to Contract	1,650	1,700	1,750	1,794
Income Outside Contract	166	90	760	796
TOTAL	**1,816**	**1,790**	**2,510**	**2,590**

EXPENDITURE (in kCHF)

Infrastructure Expenses

Energy and Consumables

Maintenance & Running Costs

Personnel

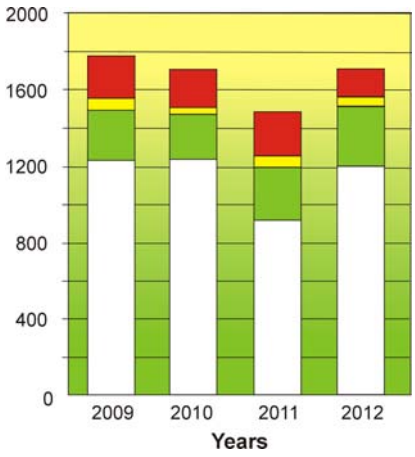

EXPENDITURE in kCHF	2009	2010	2011	2012
Personnel	1,238	1,240	1,082	1,213
Maintenance and Running Costs	263	233	208	276
Energy and Consumables	65	42	41	34
Infrastructure Expenses	220	200	155	169
TOTAL	**1,786**	**1,715**	**1,486**	**1,692**

Organization Chart of the SNBL

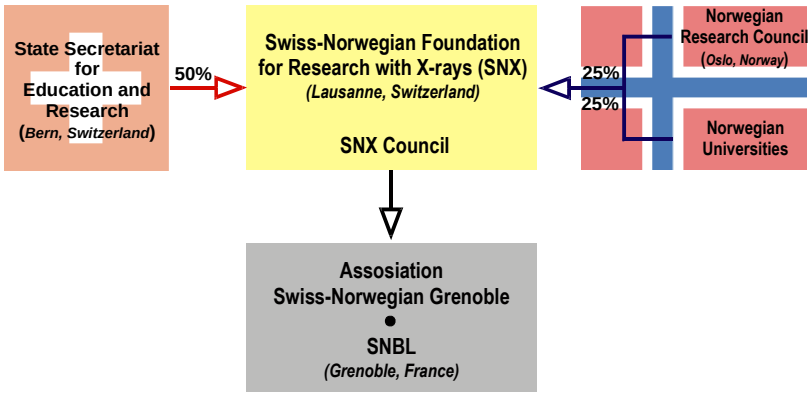

SNX Council

MEMBERS

Prof. G. Chapuis – Chairman	EPF Lausanne, Switzerland
Prof. H.Fjellvag – Vice-Chairman	University of Oslo, Norway
Prof. M.Ronning	NTNU, Trondheim, Norway
Prof. J. van Bokhoven	ETH Zurich / PSI, Switzerland
Prof. P.Macchi	University of Bern, Switzerland
Prof. B.Hauback	IFE, Kjeller, Norway
Dr. V. Dmitriev	SNBL, Grenoble, France

ADVISERS

Dr. A.M. Hundere	The Research Council of Norway
Dr. M. Steinacher	State Secretariat for Education and Research, Switzerland

SNBL Staff

(2011-2012)

Dr. V. Dmitriev – Project Director

A-station	*B-station*
Dr. P. Pattison – BL responsable	**H. Emerich** – BL responsable
Dr. D. Chernyshov – BL scientist	**Dr. W. van Beek** – BL scientist
Dr. V. Dyadkin – BL scientist	**Dr. P. Abdala** – BL scientist

Ch. Heurtebise – Administrative manager

G. Wiker – Senior technician

PUBLICATIONS

Publication Rate since start-up of SNBL

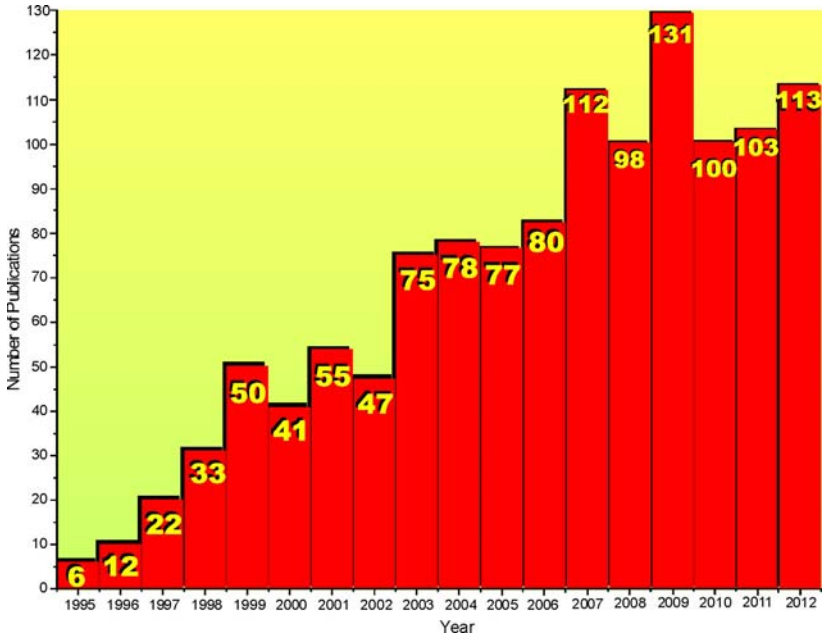

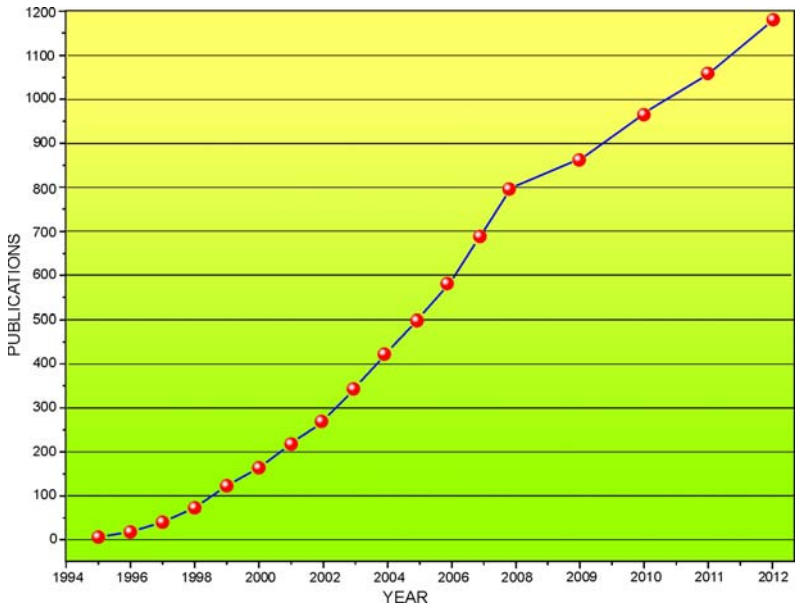

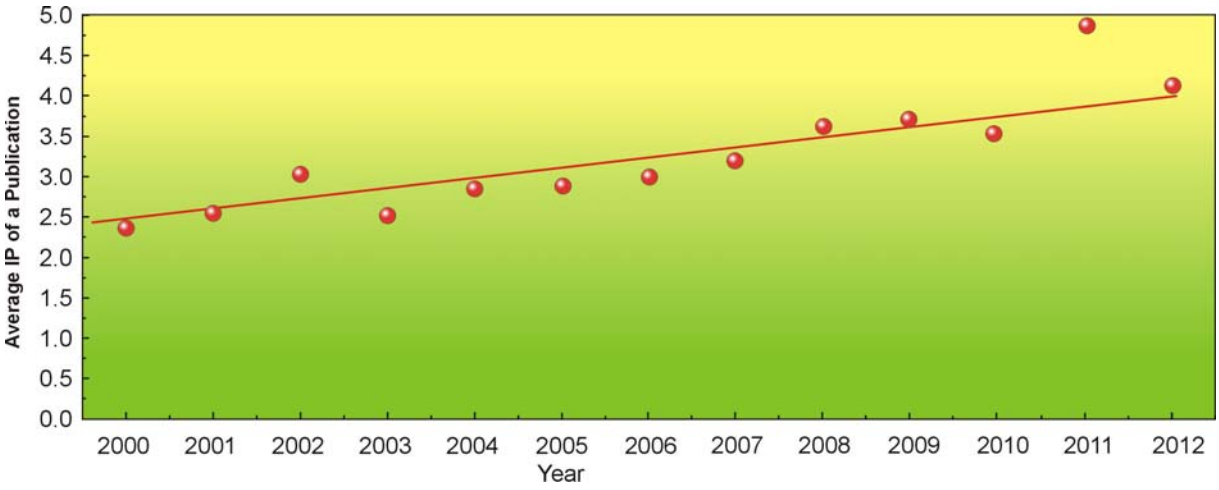

Impact factor of the "average journal" paper produced by the SNBL Users. Straight line is the best least-square fit.

List of Publications

2011

1. **Aboshyan-Sorgho, L., Besnard, C., Pattison, Ph., Kittilstved, K.R., Aebischer, A. et al**. *Near-Infrared ->Visible Light Upconversion in a Molecular Trinuclear d–f–d Complex* Angewandte Chem. Int. Ed., **50**, 18, 4108-4112, 2011
2. **Amieiro-Fonseca, A., Ellis, S. R., Nuttall, C. J., Hayden, B. E., Guerin, S., Purdy, G. et al.** *A multidisciplinary combinatorial approach for tuning promising hydrogen storage materials towards automotive applications* Faraday Discuss., **151**, 369-384, 2011
3. **Andersson, O., Filinchuk, Y., Dmitriev, V., Quwar, I., Talyzin, A., Sundqvist, B.** *Phase coexistence and hysteresis effects in the pressure-temperature phase diagram of NH_3BH_3* Phys. Rev. B **84**, 024115-024126, 2011
4. **Arletti, R., Vezzalini, G., Morsli, A., Di Renzo, F., Dmitriev, V., Quartieri, S.** *Elastic behaviour of MFI-type zeolites: 1- Compressibility of Na-ZSM-5 in penetrating and non-penetrating media* Microp.& Mesop. Mat., **142**, 2-3, 696-707 , 2011
5. **Babanova, O. A., Soloninin, A.V., Skripov, A.V., Ravnsbæk, D.V., Jensen, T.R., Filinchuk, Y.** *Reorientational Motion in Alkali-Metal Borohydrides: NMR Data for $RbBH_4$ and $CsBH_4$ and Systematics of the Activation Energy Variations* J. Phys. Chem. C, **115**, 20, 10305–10309, 2011
6. **Barpanda, P., Ati, M., Melot, B. C., Rousse, G., Chotard, J-N., Doublet, M-L. et al.** *A 3.90 V iron-based fluorosulphate material for lithium-ion batteries crystallizing in the triplite structure* Nature Materials, **10**, 772-779, 2011
7. **Barpanda, P., Chotard, J.-N., Delacourt, Ch., Reynaud, M., Filinchuk, Y. et al.** *$LiZnSO_4F$ Made in an Ionic Liquid: A Ceramic Electrolyte Composite for Solid-State Lithium Batteries* Angewandte Chem. Int. Ed., **50**, 11, 2526-2531, 2011
8. **Borgschulte, A., Jain, A., Ramirez-Cuesta, A. J., Martelli, P., Remhof, A., Friedrichs, O. et al.** *Mobility and dynamics in the complex hydrides $LiAlH_4$ and $LiBH_4$* Faraday Discuss., **151**, 213-230, 2011
9. **Bortolotti, M., Lonardelli, I., Pepponi, G.** *Determination of the crystal structure of nifedipine form C by synchrotron powder diffraction* Acta Cryst., B **67**, 357-364, 2011

10. **Boyesen, K. L., Meneau, F., Mathisen, K**. *A combined in situ XAS/Raman and WAXS study on nanoparticulate V_2O_5 in zeolites ZSM-5 and Y* Phase Transitions, **84**, 8, 675-686, 2011
11. **Buchter, F., Lodziana, Z., Remhof, A., Mauron, Ph., Friedrichs, O. et al.** *Experimental charge density of $LiBD_4$ from maximum entropy method* Phys. Rev. B **83**, 064107- 064116, 2011
12. **Budhysutanto, W.N., Hendrikx, R.W.A., Kramer, H.J.M.** *Towards solving the crystal structure of polytype $3R_2$ Mg–Al layered double hydroxides* Applied Clay Science, **54**, 1, 77-82, 2011
13. **Cerný, R., Filinchuk, Y.** *Complex inorganic structures from powder diffraction:case of tetrahydroborates of light metals* Zeitschrift für Kristallographie, **226**, 12, 882-891, 2011
14. **Cervellino, A., Gvasaliya, S. N., Zaharko, O., Roessli, B., Rotaru, G. M., Cowley, R. A. et al.** *Diffuse scattering from the lead-based relaxor ferroelectric $PbMg_{1/3}Ta_{2/3}O_3$* J. Appl. Cryst., **44**, 603-609, 2011
15. **Chernyshov, D., Van Beek, W., Emerich, H., Milanesio, M., Urakawa, A. et al.** *Kinematic diffraction on a structure with periodically varying scattering function* Acta Cryst., A 67, **4**, 327-335, 2011
16. **Chong, Ch., Itoi, M., Boukheddaden, K., Codjovi, E., Rotaru, A., Varret, F., Frye, F.A. et al.** *Talham Metastable state of the photomagnetic Prussian blue analog $K_{0.3}Co[Fe(CN)_6]_{0.77}\cdot 3.6H_2O$ investigated by various techniques* Phys. Rev. B **84**, 144102-144114, 2011
17. **Chukanov, N. V., Pekov, I. V., Jonsson, E., Zubkova, N., V., Filinchuk, Y. et al.** *Langbanshyttanite, a new low-temperature arsenate mineral with a novel structure from Langban, Sweden* Eur. J. Mineralogy, **23**, 4, 675-681, 2011
18. **Degryse, F., Voegelin, A., Jacquat, O., Kretzschmar, R., Smolders, E.** *Characterization of zinc in contaminated soils: complementary insights from isotopic exchange, batch extractions and XAFS spectroscopy* Eur. J. Soil Science, **62**, 2, 318-330, 2011
19. **Deledda, S., Hauback, B. C.** *Hydride formation in Mg-based systems processed by reactive milling* Faraday Discuss., **151**, 315-326, 2011
20. **Deloudi, S., Fleischer, F., Steurer, W.** *Unifying cluster-based structure models of decagonal Al-Co-Ni, Al-Co-Cu and Al-Fe-Ni* Acta Cryst., B **67**, 1-17, 2011
21. **Denys, R.V., Yartys, V.A.** *Effect of magnesium on the crystal structure and thermodynamics of the $La_{3-x}Mg_xNi_9$ hydrides* J. Alloys & Compounds, **509**, 2, S540-S548, 2011
22. **Dyadkin, V. A., Grigoriev, S. V., Menzel, D., Chernyshov, D., Dmitriev, V., Schoenes, J. et al**. *Control of chirality of transition-metal monosilicides by the Czochralski method* Phys. Rev. B **84**, 014435-014440, 2011
23. **Dilnesa, B.Z., Lothenbach, B., Le Saout, G., Renaudin, G., Mesbah, A., Filinchuk, Y. et al**. *Iron in carbonate containing AFm phases* Cement & Concrete Research, **41**, 3, 311-323 , 2011
24. **Fijalkowski, K. J., Genova, R. V., Filinchuk, Y., Budzianowski, A., Derzsi, M. et al.** *$Na[Li(NH_2BH_3)_2]$ – the first mixed-cation amidoborane with unusual crystal structure* Dalton Trans., **40**, 4407-4413 , 2011
25. **Filinchuk, Y., Richter, B., Jensen, T.R., Dmitriev, V., Chernyshov, D., Hagemann, H.** *Porous and Dense Magnesium Borohydride Frameworks: Synthesis, Stability, and Reversible Absorption of Guest Species* Angewandte Chem. Int. Ed., **50**, 47, 11162–11166, 2011
26. **Fonneløp, J. E., Corno, M., Grove, H., Pinatel, E., Sørby, M. H., Ugliengo, P., Baricco, M., Hauback, B. C.** *Experimental and computational investigations on the AlH_3/AlF_3 system* J. Alloys & Compounds, **509**, 1, 10-14, 2011
27. **Fonneløp, J. E., Løvvik, O. M., Sørby, M.H., Brinks, H.W., Hauback, B.C.** *Adjustment of the decomposition path for Na_2LiAlH_6 by TiF_3 addition* Int. J. Hydrogen Energy, **36**, 19, 12279-12285, 2011
28. **Frommen, Ch., Sørby, M. H., Ravindran, P., Vajeeston, P., Fjellvåg, H., Hauback, B.C.** *Synthesis, Crystal Structure and Thermal Properties of the First Mixed-Metal and Anion-Substituted Rare Earth Borohydride $LiCe(BH_4)_3Cl$* J. Phys. Chem. C, **115**, 47, 23591–23602, 2011
29. **Frommer, J., Voegelin, A., Dittmar, J., Marcus, M. A., Kretzschmar, R.** *Biogeochemical processes and arsenic enrichment around rice roots in paddy soil: results from micro-focused X-ray spectroscopy* Eur. J. Soil Science, **62**, 2, 305-317, 2011
30. **Grigoryeva, N. A., Mistonov, A. A., Napolskii, K. S., Sapoletova, N. A., Eliseev, A. A. et al.** *Magnetic topology of Co-based inverse opal-like structures* Phys. Rev. B **84**, 064405-064418, 2011

31. **Grove, H., Løvvik, O.M., Huang, W., Opalka, S.M., Heyn, R. H., Hauback, B.C.** *Decomposition of lithium magnesium aluminum hydride* Int. J. Hydrogen Energy, **36**, 13, 7602-7611, 2011
32. **Hagemann, H., D'Anna, V., Rapin, J.-Ph., Cerný, R., Filinchuk, Y., Kimd, K. Ch. et al.** *New fundamental Experimental Studies on* α-$Mg(BH_4)_2$ *and other borohydrides* J. Alloys & Compounds, **509**, 2, S688-S690, 2011
33. **Hersleth, H.-P., Andersson, K. K.** *How different oxidation states of crystalline myoglobin are influenced by X-rays* Bioch. & Bioph. Acta (BBA) - Proteins & Proteomics, **1814**, 6, 785-796, 2011
34. **Horcajada, P., Salles, F., Wuttke, S., Devic, Th., Heurtaux, D., Maurin, G., Vimont, A. et al.** *How Linker's Modification Controls Swelling Properties of Highly Flexible Iron(III) Dicarboxylates MIL-88* J. Am. Chem. Soc., **133**, 44, 17839–17847, 2011
35. **Hutanu, V., Sazonov, A., Murakawa, H., Tokura, Y., Náfrádi, B., Chernyshov, D.** *Symmetry and structure of multiferroic* $Ba_2CoGe_2O_7$ Phys. Rev. B **84**, 212101-212105, 2011
36. **Icli, B., Sheepwash, E., Riis-Johannessen, Th., Schenk, K., Filinchuk, Y., Scopelliti, R., Severin, K.** *Dative boron–nitrogen bonds in structural supramolecular chemistry: multicomponent assembly of prismatic organic cages* Chem. Sci., **2**, 1719-1721, 2011
37. **Jacob, I., Deledda, S., Bereznitsky, M., Yeheskel, O., Filipek, S.M., Mogilyanski, D., Kimmel, G., Hauback** *Can reduced size of metals induce hydrogen absorption:* $ZrAl_2$ *case* J. Alloys & Compounds, **509**, 2, S794-S796, 2011
38. **Jørgensen, M. R. V., Clausen, H. F., Christensen, M., Poulsen, R. D., Overgaard, J., Iversen, B. B**. *Crystal Structures and Physical Properties of Three New Manganese-Based Coordination Polymers with p-Biphenyldicarboxylic Acid Linkers* Eur. J. Inorganic Chem.,2011, **4**, 549–555, 2011
39. **Kaegi, R., Voegelin, A., Sinnet, B., Zuleeg, S., Hagendorfer, H., Burkhardt, M., Siegrist, H.** *Behavior of Metallic Silver Nanoparticles in a Pilot Wastewater Treatment Plant* Environ. Sci. Technol., **45**, 9, 3902–3908, 2011
40. **Karaca, H., Safonova, O., Chambrey, S., Fongarland, P., Roussel, P., Griboval-Constant, A. et al.** Structure and catalytic performance of Pt-promoted alumina-supported cobalt catalysts under realistic conditions of Fischer–Tropsch synthesis J. Catalysis, **277**,14-26, 2011
41. **Kristiansen, T., Mathisen, K., Einarsrud, M.-A., Bjoergen, M., Nicholson, D. G.** *Single-Site Copper by Incorporation in Ambient Pressure Dried Silica Aerogel and Xerogel Systems: An XAS study* J. Phys. Chem. C, **115**, 39, 19260–19268, 2011
42. **Kruk, I., Zajdel, P., Van Beek,W., Bakaimi, I., Lappas, A., Stock, Ch., Green, M. A.** *Coupled Commensurate Cation and Charge Modulation in the Tunneled Structure,* $Na_{0.40(2)}MnO_2$ J. Am. Chem. Soc., **133**, 35, 13950–13956, 2011
43. **Krzton-Maziopa, A., Pomjakushina, E., Pomjakushin, V., Sheptyakov, D., Chernyshov, D., Svitlyk, V. et al.** *The synthesis, and crystal and magnetic structure of the iron selenide* $BaFe_2Se_3$ *with possible superconductivity at* T_c *= 11 K* J. Phys.: Condens. Matter, **23**, 40, 2201-2208, 2011
44. **Kuczera, P., Wolny, J., Fleischer, F., Steurer, W.** *Structure refinement of decagonal Al-Ni-Co, superstructure type I* Philosophical Magazine, **91**, 19-21, 2500-2509, 2011
45. **Kverneland, A., Hansen, V., Thorkildsen, G., Larsen, H.B., Pattison P. et al.** *Transformations and structures in the Al-Zn-Mg alloy system. A diffraction study using synchrotron radiation and electron precession* Materials Science and Engineering: A, **528**, 880-887, 2011
46. **Leclerc, H., Devic, Th., Devautour-Vinot, S., Bazin, Ph., Audebrand, N. et al.** *Influence of the Oxidation State of the Metal Center on the Flexibility and Adsorption Properties of a Porous MOF: MIL-47 (V)* J. Phys. Chem. C, **115**, 40, 19828–19840, 2011
47. **Lejeune, M., Grosshans, Ph., Berclaz, Th., Sidorenkova, H., Besnard, C., Pattison, Ph., Geoffroy, M.** *Role of the aromatic bridge on radical ions formation during reduction of diphosphaalkenes* New J. Chem., **35**, 2510-2520, 2011
48. **Leininger, Ph., Chernyshov, D., Bosak, A., Berger, H., Inosov, D. S.** *Competing charge density waves and temperature-dependent nesting in 2H-*$TaSe_2$ Phys. Rev. B **83**, 233101-233105, 2011
49. **Leontyev, I. N. ., Belenov, S. V., Guterman, V. E., Haghi-Ashtiani, P., Shaganov, A. P., Dkhil, B.** *Catalytic Activity of Carbon-Supported Pt Nanoelectrocatalysts. Why Reducing the Size of Pt Nanoparticles is Not Always Beneficial* J. Phys. Chem. C, **115**, 13, 5429–5434, 2011

50. **Leontyev, I., Yuzyuk, Yu., Janolin, P-E., El-Marssi, M., Chernyshov, D ., Dmitriev, V. et al.** *Orthorhombic polar Nd-doped $BiFeO_3$ thin film on MgO substrate* J. Phys.: Condens. Matter, **23**, 33, 2201-2206, 2011
51. **Lindemann, I., Ferrer, R. D., Dunsch, L., Cerný, R., Hagemann, H., D'Anna, V., Filinchuk, Y. et al.** *Novel sodium aluminium borohydride containing the complex anion $[Al(BH_4,Cl)_4]$-* Faraday Discuss., **151**, 231-242, 2011
52. **Liu, L., Yang, J., Li, J., Dong, J., Šišak, D., Luzzatto, M., McCusker, L. B.** *Ionothermal Synthesis and Structure Analysis of an Open-Framework Zirconium Phosphate with a High CO2/CH4 Adsorption Ratio* Angewandte Chem. Int. Ed., **50**, 35, 8139-8142, 2011
53. **Lototsky, M.V., Williams, M., Yartys, V.A., Klochko, Ye.V., Linkov, V.M.** *Surface-Modified Advanced Hydrogen Storage Alloys for Hydrogen Separation and Purification* J. Alloys & Compounds, **509**, 2, S555-S561, 2011
54. **Martinelli, A., Palenzona, A., Tropeano, M.., Putti, M., Ferdeghini, C., Profeta, G., Emerich, H.** *Retention of the Tetragonal to Orthorhombic Structural Transition in F-Substituted SmFeAsO: A New Phase Diagram for $SmFeAs(O_{1-x}F_x)$* Phys. Rev. Lett., **106**, 227001-227005, 2011
55. **Martis, V., Nikitenko, S., Sen, S., Sankar, G., Van Beek, W., Filinchuk, Y., Snigireva, I., Bras, W.** *Effects of X-rays on crystal nucleation in lithium disilicate* Cryst. Growth Des., **11**, 7, 2858–2865, 2011
56. **McCusker, L., Baerlocher, Ch., Burton, A., Zones, S.** *A re-examination of the structure of the germanosilicate zeolite SSZ-77* Solid State Sciences, **13**, 4, 800-805, 2011
57. **Meersman, F., Quesada Cabrera, R., McMillan, P. F., Dmitriev, V.** *Structural and Mechanical Properties of TTR105-115 Amyloid Fibrils from Compression Experiments* Biophysical J., **100**, 1, 193-197, 2011
58. **Mesbah, A., François, M., Cau-dit-Coumes, C., Frizon, F., Filinchuk, Y., Leroux, F. et al.** *Crystal structure of Kuzel's salt $3CaO{\cdot}Al_2O_3{\cdot}1/2CaSO_4{\cdot}1/2CaCl_2{\cdot}11H_2O$ determined by synchrotron powder diffraction* Cement & Concrete Res., **41**, 5, 504-509, 2011
59. **Mondal, S., Van Smaalen, S., Schönleber, A., Filinchuk, Y., Chernyshov, D. et al.** *Electron-Deficient and Polycenter Bonds in the High-Pressure y-B_{28} Phase of Boron* Phys. Rev. Lett., **106**, 215502- 215506, 2011
60. **Nagalakshmi, R., Kulkarni, R., Dhar, S.K., Thamizhavel, A., Krishnakumars, V. et al.** Crystal growth and structure determination of the novel tetragonal compound Ce_2RhGa_{12} Chem. Met. Alloys, **4**, 2011
61. **Napolskii, K. S., Roslyakov, I.V., Eliseev, A. A., Petukhov, D. I., Lukashin, A.V., Chen, Sh.-F., Liu, Ch.-P., Tsirlina, G.A.** *Tuning the microstructure and functional properties of metal nanowire arrays via deposition potential* Electrochimica Acta, **56**, 5, 1, 2378-2384 , 2011
62. **Narygina, O., Dubrovinsky, L. S., Miyajima, N., McCammon, C. A., Kantor, I. Yu., Mezouar, M., Prakapenka, V. B., Dubrovinskaia, N. A., Dmitriev, V.** *Phase relations in Fe–Ni–C system at high pressures and temperatures* Phys. Chem. Minerals., **38**, 3, 203-214, 2011
63. **Neuhausen, Ch., Pattison, Ph., Schiltz, M.** *A new polymorph of dicesium tetracyanoplatinate monohydrate with unusual platinum stacking* CrystEngComm, **13**, 430-432 , 2011
64. **Olsen, J.E., Sørby, M.H., Hauback, B.C.** *Chloride-substitution in sodium borohydride* J. Alloys & Compounds, **509**, 24, L228-L231, 2011
65. **Palatinus, L., Fleischer, F., Pattison, P., Weber, T., Steurer, W.** *Ab initio reconstruction of difference densities by charge flipping* Acta Cryst., A**67**, 9-20, 2011
66. **Palin, L., Croce, G., Viterbo, D., Milanesio, M.** *Monitoring the Formation of H-MCM-22 by a Combined XRPD and Computational Study of the Decomposition of the Structure Directing Agent* Chem. Mater., **23**, 22, 4900–4909, 2011
67. **Paul-Boncour, V., Filipek, S.M., Sato, R., Wierzbicki, R., André, G., Porcher, F., Reissner, M., Wiesingerd, G.** *Structural and magnetic properties of $RMn_{2-x}Fe_xD_6$ compounds (R=Y, Er; x≤0.2) synthesized under high deuterium pressure* J. Solid State Chemistry, **184**, 2, 463-469 , 2011
68. **Podder, A. S., Lonardelli, I., Molinari, A., Bhadeshia, H. K. D. H.** *Thermal stability of retained austenite in bainitic steel: an in situ study* Proc. R. Soc. A, **15**, 2011
69. **Poletaev, A.A., Denys, R.V., Solberg, J.K., Tarasov, B.P., Yartys, V.A.** *Microstructural optimization of $LaMg_{12}$ alloy for hydrogen storage* J. Alloys & Compounds, **509**, 2, S633-S639, 2010
70. **Pomjakushin, V. Yu., Sheptyakov, D. V., Pomjakushina, E. V., Krzton-Maziopa, A., Conder, K., Chernyshov, D., Svitlyk, V. et al.** *Iron-vacancy superstructure and possible*

room-temperature antiferromagnetic order in superconducting $Cs_yFe_{2-x}Se_2$ Phys. Rev. B, **83**, 14, 144410-144415, 2011

71. **Prigent, J., Joubert, J.-M.** *The phase diagrams of the ternary systems La–Ni–M (M = Re, Ru, Os, Rh, Ir, Pd, Ag, Au) in the La-poor region* Intermetallics, **19**, 295-301, 2011
72. **Quartieri, S., Montagna, G., Arletti, R., Vezzalini, G.** *Elastic behavior of MFI-type zeolites: Compressibility of H-ZSM-5 in penetrating and non-penetrating media* J. Solid State Chem., **184**, 6, 1505-1516, 2011
73. **Quesada Cabrera, R., Meersman, F., McMillan, P.F., Dmitriev, V.** *Nanomechanical and Structural Properties of Native Cellulose Under Compressive Stress* Biomacromolecules, **2,** 6, 2178–2183, 2011
74. **Quesada Cabrera, R., Sella, A., Bailey, E., Leynaud, O., McMillan, P.F.** *High-pressure synthesis and structural behavior of sodium orthonitrate* Na_3NO_4 J. Solid State Chem., **184**, 4, 915-920, 2011
75. **Ramsahye, N.A., Trung, T.K., Bourrelly, S., Yang, Q., Devic, Th., Maurin, G. et al.** *Influence of the Organic Ligand Functionalization on the Breathing of the Porous Iron Terephthalate Metal Organic Framework Type Material upon Hydrocarbon Adsorption* J. Phys. Chem. C, **115**, 38, 18683–18695, 2011
76. **Riabov, A.B., Denys, R.V., Maehlen, J.P., Yartys, V.A.** *Synchrotron diffraction studies and thermodynamics of hydrogen absorption–desorption processes in* $La_{0.5}Ce_{0.5}Ni_4Co$ J. Alloys & Compounds, **509**, 2, S844-S848, 2011
77. **Riktor, M. D., Filinchuk, Y., Vajeeston, P., Bardají, E. G., Fichtner, M., Fjellvåg, H., Sørby, M. H., Hauback, B. C**. *The crystal structure of the first borohydride borate,* $Ca_3(BD_4)_3(BO_3)$ J. Mater. Chem., **21**, 7188-7193, 2011
78. **Rude, L. H., Filinchuk, Y., Sørby, M.H., Hauback, B.C., Besenbacher, F., Jensen, T.R.** *Anion Substitution in* $Ca(BH_4)_2$-CaI_2*: Synthesis, Structure and Stability of Three New Compounds* J. Phys. Chem. C, **115**, 15, 7768–7777, 2011
79. **Rude, L. H., Groppo, E., Arnbjerg, L. M., Ravnsbæk, D. B., Malmkjæras, R. A., Filinchuk, Y. et al.** *Iodide substitution in lithium borohydride,* $LiBH_4$-*LiI* J. Alloys & Compounds, **509**, 33, 8299-8305, 2011
80. **Rude, L.H., Zavorotynska, O., Arnbjerg, L.M., Ravnsbæk, D.B., Malmkjær, R.A. et al.** *Bromide substitution in lithium borohydride,* $LiBH_4$–*LiBr* Int. J. Hydrogen Energy, **36**, 24, 15664-15672, 2011
81. **Sadeqzadeh, M., Karaca, H., Safonova, O.V., Fongarland, P., Chambrey, S., Roussel, P.,A., Griboval-Constant, P., Lacroix, M. et al.** *Identification of the active species in the working alumina-supported cobalt catalyst under various conditions of Fischer–Tropsch synthesis* Catalysis Today, **164**, 1, 62-67, 2011
82. **Salvadó, N., Butí, S., Labrador, A., Cinque, G., Emerich, H., Pradell,T.** *SR-XRD and SR-FTIR study of the alteration of silver foils in medieval paintings* Anal. Bioanal. Chem., **399**, 9, 3041-3052, 2011
83. **Schärer, M. A., Eliot, A.C., Grütter, M. G., Capitani, G.** *Structural basis for reduced activity of 1-aminocyclopropane-1-carboxylate synthase affected by a mutation linked to andromonoecy* FEBS Letters, **585**, 111-114, 2011
84. **Schaub, P. Weber, T., Steurer, W.** *Analysis and modelling of structural disorder by the use of the three-dimensional pair distribution function method exemplified by the disordered twofold superstructure of decagonal Al-Cu-Co* J. Appl. Cryst., **44**, 1, 134–149, 2011
85. **Serra-Crespo, P., Ramos-Fernandez, E. V., Gascon, J., Kapteijn, F.** *Synthesis and Characterization of an Amino Functionalized MIL-101(Al): Separation and Catalytic Properties* Chem. Mater., **23**, 10, 2565–2572, 2011
86. **Skorpa, R., Bordiga, S., Bleken, F., Olsbye, U., Arstad, B., Tolchard, J., Mathisen, K., et al.** *Assessing the surface sites of the large pore 3-dimensional microporous material H-ITQ-7 using FT-IR spectroscopy and molecular probes* Microp.& Mesop. Mater., **141**, 1-3, 146-156, 2011
87. **Skrzypski, J., Bezverkhyy, I., Safonova, O., Bellat, J.-P**. *2.8NiO-*$H_{1.8}Ni_{0.6}(OH)MoO_4$ *- novel nanocomposite material for the reactive adsorption of sulfur-containing molecules at moderate temperature* Applied Catalysis B: Environmental, **106**, 3-4, 460-468, 2011
88. **Song, H., Sjåstad, A. O., Fjellvåg, H., Okamoto, H., Vistad, Ø. B., Arstad, B., Norby, P.** *Exfoliation and thermal transformations of Nb-substituted layered titanates* J. Solid State Chemistry, **184**, 12, 4900–4909, 2011

89. **Stare,K., Cerný, R., Skapin, S.D., Suvorov, D., Meden, A.** *Crystal Structures of $CaLa_8Ti_9O_{31}$ and $Ca_2La_4Ti_6O_{20}$ Determined from Powder Diffraction Data* Acta Chim. Slov., **58**, 465–470, 2011
90. **Suwarno, S., Solberg, J.K., Yartys, V.A., Krogh, B.** *Hydrogenation and Microstructural Study of Melt-Spun $Ti_{0.8}V_{0.2}$* J. Alloys & Compounds, **509**, 2, S775-S778, 2011
91. **Svitlyk, V., Chernyshov, D., Pomjakushina, E., Krzton-Maziopa, A., Conder, K., Pomjakushin, V., Dmitriev, V.** *Temperature and Pressure Evolution of the Crystal Structure of $A_x(Fe_{1-y}Se)_2$ (A = Cs, Rb, K) Studied by Synchrotron Powder Diffraction* Inorg. Chem., **50**, 21, 10703–10708, 2011
92. **Talyzin, A. V., Luzan, S. M., Leifer, K., Akhtar, S., Fetzer, J., Cataldo, F. et al.** *Coronene Fusion by Heat Treatment: Road to Nanographenes* J. Phys. Chem. C, **115**, 27, 13207–1321, 2011
93. **Talyzin, A.V., Luzan, S.M., Szabó, T., Chernyshev, D., Dmitriev, V.** *Temperature dependent structural breathing of hydrated graphite oxide in H_2O* Carbon, **49**, 6, 1894-1899, 2011
94. **Talyzin, A. V. , Sundqvist, B., Szab, T., Dmitriev, V.** *Structural Breathing of Graphite Oxide Pressurized in Basic and Acidic Solutions* J. Phys. Chem. Lett., **2**, 4, 309–313, 2011
95. **Tew, M. W., Emerich, H., van Bokhoven, J.A.** *Formation and Characterization of PdZn Alloy: A Very Selective Catalyst for Alkyne Semihydrogenation* J. Phys. Chem. C, **115**, 17, 8457–8465, 2011
96. **Tong, L. H., Gune, L., Williams, A.F.** *Pentasubstituted Ferrocene and Dirhodium(II) Tetracarboxylate as Building Blocks for Discrete Fullerene-Like and Extended Supramolecular Structures* Inorg. Chem., **50**, 6, 2450–2457, 2011
97. **Trung, Th. Kh., Déroche, I., Rivera, A., Yang, Q., Yot, P., Ramsahye, N. et al.** *Hydrocarbon adsorption in the isostructural Metal Organic Frameworks MIL-53 (Cr) and MIL-47 (V)* Microp. & Mesop. Materials, **140**, 1-3, 114-119, 2011
98. **Urakawa, A., Van Beek, W., Monrabal-Capilla, M., Galn-Mascars, J.R., Palin, L., Milanesio, M.** *Combined, Modulation Enhanced X-ray Powder Diffraction and Raman Spectroscopic Study of Structural Transitions in the Spin Crossover Material [Fe(Htrz)2(trz)](BF4)* J. Phys. Chem. C, **115**, 4, 1323–1329, 2011
99. **Vakhrushev, S. B., Shaganov, A.P., Dkhil, B., Lebolock, D., Ouvada, K.** *Study of the formation processes of a domain nanostructure in relaxor ferroelectrics* Physics of Particles and Nuclei Letters, **8**, 10, 1061-1062, 2011
100. **Van Beek, W., Safonova, O.V., Wiker, G., Emerich, H.** *SNBL, a dedicated beamline for combined in situ X-ray diffraction, X-ray absorption and Raman scattering experiments* Phase Transitions, **84**, 8, 726-732, 2011
101. **Voegelin, A., Jacquat, O., Pfister, S., Barmettler, K., Scheinost, A.S., Kretzschmar, R.** *Time-Dependent Changes of Zinc Speciation in Four Soils Contaminated with Zincite or Sphalerite* Environ. Sci. Technol., **45**, 1, 255–261, 2011
102. **Vullum, P. E., Pitt, M., Walmsley, J., Hauback, B., Holmestad, R.** *Equation TEM characterization of pure and transition metal enhanced $NaAlH_4$* J. Alloys & Compounds, **509**, 2, 281-289, 2011
103. **Walspurger, S., de Munck, S., Cobden, P.D., Haije, W.G., van den Brink, R.W., Safonova, O.V.** *Correlation between structural rearrangement of hydrotalcite-type materials and CO_2 sorption processes under pre-combustion decarbonisation conditions* Energy Procedia, **4**, 1162-1167, 2011
104. **Wang, J., Schenk, K., Carvalho, A., Wylie-van Eerd, B. et al.** *Structure Determination and Compositional Modification of Body-Centered Tetragonal PX-Phase Lead Titanate* Chem. Mater., **23**, 10, 2529–2535, 2011
105. **Wiersum, A. D., Soubeyrand-Lenoir, E., Yang, Q., Moulin, B., Guillerm, V. et al.** *An Evaluation of UiO-66 for Gas-Based Applications* Chemistry – An Asian J., **6**, 12, 3270–3280, 2011
106. **Wragg, D.S., Akporiaye, D., Fjellvåg, H.** *Direct observation of catalyst behaviour under real working conditions with X-ray diffraction: Comparing SAPO-18 and SAPO-34 methanol to olefin catalysts* J. Catalysis, **279,** 2, 397-402, 2011
107. **Xie, D., Baerlocher, Ch., McCusker, L.B.** *Using phases retrieved from two-dimensional projections to facilitate structure solution from X-ray powder diffraction data* J. Appl. Cryst., **44**, 5, 2011
108. **Xie, D., McCusker, L.B., Baerlocher, Ch.** *Structure of the borosilicate zeolite catalyst SSZ-82 solved using 2D-XPD charge flipping* J. Am. Chem. Soc.,**133**, 50, 20604–20610, 2011

109. **Yartys, V.A., Denys, R.V., Webb, C.J., Mæhlen, J.P., Gray, MacA., Blach, T. et al.** *High pressure in situ diffraction studies of metal-hydrogen systems* J. Alloys & Compounds, **509**, 2, S817-S822, 2011
110. **Zhang, J., Cerný, R., Villeroy, B., Godart, C., Chandra, D., Latroche, M.** *$Li_{3-x}M_xN$ (M = Co, Ni) synthesized by Spark Plasma Sintering for hydrogen storage* J. Alloys & Compounds, **509**, 2, S732-S735, 2011

2012

1. **Abdala, P., Safonova, O., Wiker, G., Van Beek, W., Emerich, H., Van Bokhoven, J. et al.** Scientific Opportunities for Heterogeneous Catalysis Research at the SuperXAS and SNBL Beam Lines CHIMIA Int. J. Chemistry, **66**, 9, 699-705, 2012
2. **Afanasiev, P.** *Snapshots of ZnO Formation in Molten Salt: Hollow Microtubules Generated by Oriented Attachment and Kirkendall Effect* J. Phys. Chem. C, **116**, 3 2371-2381, 2012
3. **Aimoz, L., Taviot-Gueho, Ch., Churakov, S.V., Chukalina, M., Daehn, R. et al.** *Anion and Cation Order in Iodide-Bearing Zn/Mg-Al Layered Double Hydroxides* J. Phys. Chem. C, **116**, 9, 5460-5475, 2012
4. **Aimoz, L., Wieland, E., Taviot-Gueho, Ch., Daehn, R., Vespa, M., Churakov, S.V.** *Structural insight into iodide uptake by AFm phases* Environ. Sci. Technol., **46**,7,3874-3881, 2012

5. **Alcantara, K.S., Lopez, J.R., Bösenberg, U., Saldan, I., Pistidda, C., Requejo, F. et al.** *3CaH2+4MgB2+CaF2 Reactive Hydride Composite as a Potential Hydrogen Storage Material: Hydrogenation and Dehydrogenation Pathway* J. Phys. Chem. C, **116**,12, 7207-7212, 2012
6. **Arakcheeva, A., Logvinovich, D., Chapuis, G., Morozov, V., Eliseeva, S., Bünzli, J.-C., Pattison, P.** *The luminescence of $Na_xEu^{3+}{}_{(2-x)/3}MoO_4$ scheelites depends on the number of Eu-clusters occurring in their incommensurately modulated structure* Chem. Sci., **3**, 384-390, 2012
7. **Arnbjerg, L. M., Jensen, T. R.** *New compounds in the potassium-aluminium-hydrogen system observed during release and uptake of hydrogen* Int. J. Hydrogen Energy, **37**,1, 345-356, 2012
8. **Bellussi, G., Montanari, E., Di Paola, E., Millini, R., Carati, A., Rizzo, C., O'Neil Parker Jr., W. et al.** *ECS-3: A Crystalline Hybrid Organic–Inorganic Aluminosilicate with Open Porosity* Angewandte Chem. Int. Ed., **51**, 3, 666-669, 2012
9. **Bezverkhyy, I., Skrzypski, J., Safonova, O., Bellat, J.-P.** *Sulfidation Mechanism of Pure and Cu-Doped ZnO Nanoparticles at Moderate Temperature: TEM and In Situ XRD Studies* J. Phys. Chem. C, **116**, 27, 14423-14430, 2012
10. **Bora, D.K., Braun, A., Erat, S., Safonova, O., Graule, Th., Constable, E.C.** *Evolution of structural properties of iron oxide nano particles during temperature treatment from 250°C – 900°C: X-ray diffraction and Fe K-shell pre-edge X-ray absorption study* Current Applied Physics, **12,** 3, 817-825, 2012
11. **Bosak, A., Chernyshov, D., Vakhrushev, S.** *Glass-like structure of a lead-based relaxor ferroelectric* J. Appl. Cryst., **45**, 6, 2012
12. **Bosak, A., Chernyshov, D., Vakhrushev, S., Krisch, M.** *Diffuse scattering in relaxor ferroelectrics: true three-dimensional mapping, experimental artefacts and modelling* Acta Cryst., A **68**, 1, 117-123, 2012
13. **Bosak, A., Krisch, M., Chernyshov, D., Winkler, B., Milman, V., Refson, K., Schulze-Briese, C.** *New insights into the lattice dynamics of α-quartz* Z. Kristallographie - Crystalline Mat., **227**, 2, 84-91, 2012
14. **Bozoklu, G., Gateau, Ch., Imbert, D., Pécaut, J., Robeyns, K., Filinchuk, Y. et al.** *Controlled Diastereoselective Self-Assembly and Circularly Polarized Luminescence of a Chiral Heptanuclear Europium Wheel* J. Am. Chem. Soc., **134**, 20, 8372–8375, 2012
15. **Burkovsky, R. G., Bronwald, Yu. A., Filimonov, A. V., Rudskoy, A. I., Chernyshov, D., Bosak, A. et al.** *Structural Heterogeneity and Diffuse Scattering in Morphotropic Lead Zirconate-Titanate Single Crystals* Phys. Rev. Lett., **109**, 097603-097607, 2012
16. **Bykova, E., Parakhonskiy, G., Dubrovinskaia, N., Chernyshov, D., Dubrovinsky, L.** *The crystal structure of aluminum doped β-rhombohedral boron* J. Solid State Chemistry, **194**, 188-193, 2012
17. **Caliandro, R., Chernyshov, D., Emerich, H., Milanesio, M., Palin, L., et al.** *Patterson selectivity by modulation-enhanced diffraction* J. Appl. Cryst., **45**, 3, 458-470, 2012
18. **Ceotto, M., Lo Presti, L., Cappelletti, G., Meroni, D., Spadavecchia, F., Zecca. R. et al.** *About the Nitrogen Location in Nanocrystalline N-Doped TiO_2: Combined DFT and EXAFS Approach* J. Phys. Chem. C, **116**, 2, 1764–1771, 2012

19. **Cerný, R., Ravnsbæk, D.B., Schouwink, P., Filinchuk, Y., Penin, N., Teyssier, J. et al.** *Potassium zinc borohydrides containing triangular [Zn(BH4)3]¯ and tetrahedral [Zn(BH4)xCl4-x]2¯ anions* J. Phys. Chem. C, **116**, 1, 1563-1571, 2012
20. **Cervellino, A., Gvasaliya, S. N., Roessli, B., Rotaru, G. M., Cowley, R. A. et al.** *Cube-shaped diffuse scattering and the ground state of $BaMg_{1/3}Ta_{2/3}O_3$* Phys. Rev. B **86**, 104107-104129, 2012
21. **Chakraborty, P., Bronisz, R., Besnard, C., Guénée, L., Pattison, P., Hauser, A.** Persistent Bidirectional Optical Switching in the 2D High-Spin Polymer $\{[Fe(bbtr)_3](BF_4)_2\}_\infty$ J. Am. Chem. Soc., **134,** 9, 4049-4052, 2012
22. **Chavan, S., Vitillo, J.G., Gianolio, D., Zavorotynska, O., Civalleri, B., Jakobsen, S. et al.** H_2 storage in isostructural UiO-67 and UiO-66 MOFs Phys. Chem. Chem. Phys., **14**, 1614-1626, 2012
23. **Christensen, A.N., Lebech, B.** *Investigation of the crystal structure of a basic bismuth(III) nitrate with the composition $[Bi_6O_4(OH)_4]_{0.54(1)}[Bi_6O_5(OH)_3]_{0.46(1)}(NO_3)_{5.54(1)}$* Dalton Trans., **41**, 1971-1980, 2012
24. **Conradi, M.S., Eagles, M., Sun, B., Richter, B., Jensen, T.R., Filinchuk, Y.** *NMR Investigation of Nanoporous y-$Mg(BH_4)_2$ and its Thermally-Induced Phase Changes* J. Phys. Chem. C, **116**, 24, 13033-13037, 2012
25. **Conterosito, E., Croce, G., Palin, L., Boccaleri, E., Van Beek, W., Milanesio, M.** *Crystal structure and solid-state transformations of Zn–triethanolamine–acetate complexes to ZnO* CrystEngComm, **14**, 4472-4477, 2012
26. **Couck, S., Gobechiya, E., Kirschhock, C.E.A., Serra-Crespo, P., Juan-Alcañiz, J., Joaristi, A.M. et al.** *Adsorption and Separation of Light Gases on an Amino-Functionalized Metal–Organic Framework: An Adsorption and In Situ XRD Study* ChemSusChem., **5**, 4, 740-750, 2012
27. **Deka, U., Lezcano-Gonzalez, I., Warrender, S.J., Picone, A.L., Wright, P.A., Weckhuysen, B.M. et al.** *Changing active sites in Cu-CHA catalysts: deNOx selectivity as a function of the preparation method* Microporous and Mesoporous Materials,**166**, 144-152, 2012
28. **Deka, U., Juhin, A., Eilertsen, E.A., Emerich, H., Green, M.A., Korhonen, S.T. et al.** *Confirmation of Isolated Cu^{2+} ions in SSZ-13 Zeolite as Active Sites in NH_3 - Selective Catalytic Reduction* J. Phys. Chem. C, **116**, 7, 4809-4818, 2012
29. **Denys, R.V., Poletaev, A. A., Maehlen, J.P., Solberg, J.K., Tarasov, B.P., Yartys, V.A**. *Nanostructured rapidly solidified $LaMg_{11}Ni$ alloy. II. In situ synchrotron X-ray diffraction studies of hydrogen absorption–desorption behaviours* Int. J. Hydrogen Energy, **37**, 7, 5710-5722, 2012
30. **Denys, R.V., Yartys, V.A., Webb, C.J.** *Hydrogen in $La_2MgNi_9D_{13}$: The Role of Magnesium* Inorg. Chem., **51**, 7, 4231-4238, 2012
31. **Devic, Th., Salles, F., Bourrelly, S., Moulin, B., Maurin, G., Horcajada, P. et al.** *Effect of the organic functionalization of flexible MOFs on the adsorption of CO_2* J. Mater. Chem., **22**, 10266-10273, 2012
32. **Diana, E., Chierotti, M.R., Marchese, E.M.C., Croce, G., Milanesio, M., Luigi, P.** *Stanghellini Blue and red shift hydrogen bonds in crystalline cobaltocinium complexes* New J. Chem., **36**, 1099-1107, 2012
33. **Di Bartolomeo, E., D'Epifanio, A., Pugnalini, P., Giannici, F., Longo, A., Martorana, A. et al.** *Structural analysis, phase stability and electrochemical characterization of Nb doped $BaCe_{0.9}Y_{0.1}O_{3-x}$ electrolyte for IT*-SOFCs J. Power Sources, **199**, 201–206, 2012
34. **Djerdj, I., Škapin, S.D., Ceh, M., Jaglicic, Z., Pajic, D., Kozlevcar, B., Orel, B., Orel, Z.C.** *Interplay between the structural and magnetic probes in the elucidation of the structure of a novel 2D layered $[V_4O_4(OH)_2(O_2CC_6H_4CO_2)_4]\cdot DMF$* Dalton Trans., **41**, 581-589, 2012
35. **Dmitriev, V., Chernyshov, D., Grigoriev, S., Dyadkin, V.** *A chiral link between structure and magnetism in MnSi* J. Phys.: Condens. Matter, **24**, 36, 6005-6012, 2012
36. **Eagles, M., Sun, B., Richter, B., Jensen, T.R., Filinchuk, Y., Conradi, M.S.** *NMR Investigation of Nanoporous* γ*-$Mg(BH_4)_2$ and Its Thermally Induced Phase Changes* J. Phys. Chem. C, **116**, 24, 13033-13037, 2012
37. **Fonneløp, J. E., Sartori, S., Sørby, M.H., Hauback, B.C.** *Polymorphic composition of alane after cryomilling with fluorides* J. Alloys & Compounds, **540**, 241-247, 2012
38. **Gvasaliya, S. N , Cervellino, A., Roessli, B., Rotaru, G. M., Cowley, R. A., Lushnikov, S. G. et al.** *The structure and low-energy phonons of the nonferroelectric mixed perovskite: $BaMg_{1/3}Ta_{2/3}O_3$* J. Phys.: Condens. Matter, **24**, 45, 5401-5408, 2012

39. **Guzik, M.N., Hauback, B.C., Yvon, K.** *Hydrogen atom distribution and hydrogen induced site depopulation for the $La_{2-x}Mg_xNi_7$ – H system* J. Solid State Chemistry, **186**, 9-16, 2012
40. **Hamacek, J., Besnard, C., Mehanna, N., Lacour, J.** *Tripodal europium complex with triangulenium dye: a model bifunctional metallo-organic system* Dalton Trans., **41**, 6777-6782, 2012
41. **Hansen, E. L., Hemmen, H., Fonseca, D. M., Coutant, C., Knudsen, K. D. et al.** *Swelling transition of a clay induced by heating* Scientific Reports, **2**, 618, 2012
42. **Hino, S., Fonneløp, J.E., Corno, M., Zavorotynska, O., Damin, A., Richter, B. et al.** *Halide Substitution in Magnesium Borohydride* J. Phys. Chem. C, **116**, 23, 12482-12488, 2012
43. **Jakobsen, S., Gianolio, D., Wragg, D.S., Nilsen, M.H., Emerich, H., Bordiga, S., Lamberti, C. et al.** *Structural determination of a highly stable metal-organic framework with possible application to interim radioactive waste scavenging: Hf-UiO-66* Phys. Rev. B **86**, 125429-125440, 2012
44. **Jansa, I.L., Friedrichs, O., Fichtner, M., Bardaji, E.G., Zuettel, A., Hauback, B.C**. *The Role of $Ca(BH_4)_2$ Polymorphs* J. Phys. Chem. C, **116**, 25, 13472-13479, 2012
45. **Jantsky, L., Okamoto, H., Demont, A., Fjellvåg, H.** *Tuning of Water and Hydroxide Content of Intercalated Ruddlesden–Popper-type Oxides in the $PrSr_3Co_{1.5}Fe_{1.5}O_{10-\delta}$ System* Inorg. Chem., **51**, 17, 9181-9191, 2012
46. **Kongmark, Ch., Coulter, R., Cristol, S., Rubbens, A., Pirovano, C., Löfberg, A., Sankar, G., Van Beek, W. et al.** *A Comprehensive Scenario of the Crystal Growth of γ-Bi_2MoO_6 Catalyst during Hydrothermal Synthesis* Cryst. Growth Des., **12**, 12, 5994-6003, 2012
47. **Kristiansen, T., Støvneng, J.A., Einarsrud, M.-A., Nicholson, D.G., Mathisen, K.** *There and Back Again: The Unique Nature of Copper in Ambient Pressure Dried-Silica Aerogels* J. Phys. Chem. C, **116**, 38, 20368-20379, 2012
48. **Kuczera, P., Wolny, J., Steurer, W.** *Comparative structural study of decagonal quasicrystals in the systems Al-Cu-Me (Me = Co, Rh, Ir)* Acta Cryst., B **68**, 578-589, 2012
49. **Lang, J., Gerhauser, A., Filinchuk, Y., Klassen, T., Huot, J.** *Differential Scanning Calorimetry (DSC) and Synchrotron X-ray Diffraction Study of Unmilled and Milled $LiBH_4$: A Partial Release of Hydrogen at Moderate Temperatures* Crystals., **2**, 1, 1-21, 2012
50. **Leardini, L., Quartieri, S., Martucci, A., Vezzalini, M.G., Dmitriev, V.** *Compressibility of microporous materials with CHA topology: 2. ALPO-34* Z. Kristallogr., **227**, 2012
51. **Leiros, H.-K.S., Fedøy, A.E., Leiros, I., Steen, I.H.** *The complex structures of isocitrate dehydrogenase from Clostridium thermocellum and Desulfotalea psychrophila suggest a new active site locking mechanism* FEBS Open Bio, **2**, 159-172, 2012
52. **Leontyev, I., Kuriganova, A., Kudryavtsev, Y., Dkhil, B., Smirnova, N.** *New Life of a Forgotten method: Electrochemical Route toward Highly Efficient Pt/C Catalysts for Low-Temperature Fuel Cells* Applied Catalysis A: General, **431-432**, 120-125, 2012
53. **Ley, M.B., Boulineau, S., Janot, R., Filinchuk, Y., Jensen, T.R.** *New Li Ion Conductors and Solid State Hydrogen Storage Materials: $LiM(BH_4)_3Cl$, M = La, Gd* J. Phys. Chem. C, **116**, 40, 21267-21266, 2012
54. **Ley, M.B., Ravnsbæk, D.B., Filinchuk, Y., Lee, Y.-S., Janot, R., Cho, Y.W. et al.** *$LiCe(BH_4)3Cl$, a new lithium-ion conductor and hydrogen storage material with isolated tetranuclear anionic clusters* Chem. Mater., **24,**1654-1663, 2012
55. **Llamas-Jansa, I., Aliouane, N., Deledda, S., Fonneløp, J.E., Frommen, Ch., Humphries, T. et al.** *Chloride substitution induced by mechano-chemical reactions between $NaBH_4$ and transition metal chlorides* J. Alloys and Compounds, **530**, 186-192, 2012
56. **Lonardelli, I., Bortolotti, M., Van Beek, W., Girardini, L., Zadra, M., Bhadeshia, H.K.D.H.** *Powder metallurgical nanostructured medium carbon bainitic steel: Kinetics, structure, and in situ thermal stability studies* Mat. Science and Engineering: A, **565**, 139-147, 2012
57. **Maegli, A.E., Hisatomi, T., Otal, E.H., Yoon, S., Pokrant, S., Grätzel, M., Weidenkaff, A.** *Structural and photocatalytic properties of perovskite-type $(La,Ca)Ti(O,N)_3$ prepared from A-site deficient precursors* J. Mater. Chem., **22**, 17906-17913, 2012
58. **Maercz, M., Johnsen, R.E., Dietzel, P.D.C., Fjellvåg, H.** *The iron member of the CPO-27 coordination polymer series: Synthesis, characterization, and intriguing redox properties* Microp.& Mesop. Mat., **157**, 62-74, 2012
59. **Martinelli, A., Palenzona, A., Putti, M., Ferdeghini, C.** *Microstructural evolution throughout the structural transition in 1111 oxypnictides* Phys. Rev. B **85**, 224534-224546, 2012
60. **Matam, S.K., Otal, E.H., Aguirre, M.H., Winkler, A., Ulrich, A., Rentsch, D., Weidenkaff, A., Ferr, D.** *Thermal and chemical aging of model three-way catalyst Pd/Al_2O_3 and its impact on the conversion of CNG vehicle exhaust* Catalysis Today, **184**, 1, 237-244, 2012

61. **Mathisen, K., Nilsen, M.H., Nordhei, C., Nicholson, D.G.** *Irreversible Silver(I) Interconversion in Ag:ZSM-5 and Ag:SAPO-5 by Propene and Hydrogen* J. Phys. Chem. C, **116**,1, 171-184, 2012
62. **Mikheykin, A. S., Dmitriev, V. P, Chagovets, S. V., Kuriganova, A. B., Smirnova, N. V., Leontyev, I. N**. *The compressibility of nanocrystalline Pt* Appl. Phys. Lett., **101**, 173111-173115, 2012
63. **Minkov, V.S., Boldyreva, E., Drebushchak, T.N., Gorbitz, C.H.** *Stabilizing structures of cysteine-containing crystals with respect to variations of temperature and pressure by immobilizing amino acid side chains* CrystEngComm, **14**, 5943-5954, 2012
64. **Moliner, M., Willhammar, T., Wan, W., González, J., Rey, F., Jorda, J.L. et al.** *Synthesis Design and Structure of a Multipore Zeolite with Interconnected 12- and 10-MR Channels* J. Am. Chem. Soc., **134**, 14, 6473–6478, 2012
65. **Nielsen, Th.K., Jensen, T.R.** *MgH_2–Nb_2O_5 investigated by in situ synchrotron X-ray diffraction* Int. J. Hydrogen Energy, **37**, 18, 13405-13416, 2012
66. **Nielsen, R.B., Norby, P., Kongshaug. K.O., Fejellvag, H.** *Synthesis, crystal structure and thermal properties of $Ca_6(C_{12}H_{14}O_4)_4(CO_3)(OH)_2(H2O)_x$ – a 3D inorganic hybrid material* Dalton Trans., **41**, 12082-12089, 2012
67. **Østreng, E., Nilsen, O., Fjellvåg. H.** *Optical Properties of Vanadium Pentoxide Deposited by ALD* J. Phys. Chem. C, **116**, 36, 19444-19450, 2012
68. **Ovsyannikov, S.V., Wu, X., Karkin, A.E., Shchennikov, V.V., Manthilake, G.M.** *Pressure-temperature phase diagram of Ti_2O_3 and physical properties in the golden Th_2S_3-type phase* Phys. Rev. B **86**, 024106-024120, 2012
69. **Phan, H. V., Chakraborty, P., Chen, M., Calm, Y.M., Kovnir, K. et al.** *Heteroleptic Fe^{II} Complexes of 2,2' - Biimidazole and Its Alkylated Derivatives: Spin-Crossover and Photomagnetic Behavior* Chemistry - A European J., **18**, 49, 15805-15815, 2012
70. **Parsons, S., Pattison, P., Flack, H. D.** *Analysing Friedel averages and differences* Acta Cryst., A**68**, 736-749, 2012
71. **Paun, C., Safonova, O., Szlachetko, J., Abdala, P., Nachtegaal, M., De Paiva Sa, J. et al.** *Polyhedral CeO_2 Nanoparticles: Size-Dependant Geometrical and Electronic Structure* J. Phys. Chem. C, **116**, 13, 7312-7317, 2012
72. **Pekov, I.V., Zubkova, N.V., Chukanov, N.V., Turchkova, A.G., Filinchuk, Y.E., Pushcharovsky, D.Y.** *Delhayelite and Mountainite Mineral Families: Crystal Chemical Relationship, Microporous Character and Genetic Features* Minerals as Adv. Mater. **II**, 213-219, 2012
73. **Petukhov, D. I., Eliseev, A. A., Kolesnik, I.V., Napolskii, K.S., Lukashin, A.V., Garshev, A.V. et al.** *Mechanically stable flat anodic titania membranes for gas transport applications* J. Porous Materials, **19,**1, 71-77, 2012
74. **Pinatel, U.R., Rude, L.H., Corno, M., Kragelund, M., Ugliengo, P., Jensen, T.R., Baricco, M.** *Thermodynamic Tuning of Calcium Hydride by Fluorine Substitution* Mater. Res. Soc. Symp. Proc., **1441**, 2012
75. **Pitt, M.P., Vullum, P.E., Sørby, M.H., Blanchard, D., Sulic, M.P., Emerich, H. et al**. *The location of Ti containing phases after the completion of the $NaAlH_4$ + $xTiCl_3$ milling process* J. Alloys & Compounds, **513**, 597-605, 2012
76. **Pitt, M.P., Vullum, P.E., Sørby, M.H., Emerich, H., Paskevicius, M., Buckley, C.E. et al.** *Amorphous $Al_{1-x}Ti_x$, $Al_{1-x}V_x$, and $Al_{1-x}Fe_x$ phases in the hydrogen cycled $TiCl_3$, VCl_3 and $FeCl_3$ enhanced $NaAlH_4$ systems* J. Alloys & Compounds, **521**, 112-120, 2012
77. **Pitt, M.P., Vullum, P.E., Sørby, M.H., Emerich, H., Paskevicius, M., Buckley, C.E. et al.** *Absorption Kinetics of the Transition-Metal-Chloride Enhanced $NaAlH_4$ System* J. Phys. Chem. C, **116**, 27, 14205-14217, 2012
78. **Pitt, M.P., Vullum, P.E., Sørby, M.H., Emerich, H., Paskevicius, M., Buckley, C.E. et al.** *A structural review of nanoscopic $Al_{1-x}TM_x$ phase formation in the $TMCl_n$ enhanced $NaAlH_4$ system* J. Alloys & Compounds, **527**, 16-24, 2012
79. **Pitt, M.P., Vullum, P.E., Sørby, M.H., Sulic, M.P., Emerich, H., Paskevicius, M., Buckley, C.E., Walmsley, J.C. et al.** *Functionality of the nanoscopic crystalline Al/amorphous $Al_{50}Ti_{50}$ surface embedded composite observed in the $NaAlH_4$ + $xTiCl_3$ system after milling* J. Alloys & Compounds, **514**,163-169, 2012
80. **Pitt, M.P., Vullum, E., Sørby, M.H., Emerich, H., Paskevicius, M., Webb, C.J. et al.** *Hydrogen absorption kinetics and structural features of $NaAlH_4$ enhanced with transition-metal and Ti-based nanoparticles* Int. J. Hydrogen Energy, **37**, 20, 15175-15186, 2012

81. **Poletaev, A.A., Denys, R.V., Maehlen, J.P., Solberg, J.K., Tarasov, B.R., Yartys, V.A.** *Nanostructured rapidly solidified LaMg11Ni alloy: Microstructure, crystal structure and hydrogenation properties* Int. J. Hydrogen Energy, **37**, 4, 3548-3557, 2012
82. **Pomjakushin, V. Yu., Krzton-Maziopa, A., Pomjakushina, E. V., Conder, K., Chernyshov, D., Svitlyk, V., Bosak, A.** *Intrinsic crystal phase separation in the antiferromagnetic superconductor RbyFe2-xSe2: a diffraction study* J. Phys.: Condens. Matter, **24**, 435701-435710, 2012
83. **Pregelj, M., Jeschke, H.O., Feldner, H., Valentí, R., Honecker, A., Saha-Dasgupta, T., Das, H. et al.** *Multiferroic $FeTe_2O_5Br$: Alternating spin chains with frustrated interchain interactions* Phys. Rev. B **86**, 054402-054408, 2012
84. **Quartieri, S., Arletti, R., Vezzalini, G., Di Renzo, F., Dmitriev, V.** *Elastic behavior of MFI-type zeolites: 3 – Compressibility of silicalite and mutinaite* J. Solid State Chemistry, **191**, 201-212, 2012
85. **Ravnsbæk, D.B., Ley, M.B., Lee, Y.-S., Hagemann, H., D'Anna, V., Cho, Y.W., Filinchuk, Y., Jensen, T.R.** *A mixed-cation mixed-anion borohydride $NaY(BH_4)_2Cl_2$* Int. J. Hydrogen Energy, **37**,10, 8428-8438, 2012
86. **Ravnsbæk, D.B., Sørensen, L.H., Filinchuk, Y., Besenbacher, F., Jensen, T.R.** *Screening of Metal Borohydrides by Mechanochemistry and Diffraction* Angewandte Chem. Int. Ed., **51**,15, 3582-3586, 2012
87. **Rozynek, Z., Wang, B., Fossum, J. O., Knudsen, K. D.** *Dipolar structuring of organically modified fluorohectorite clay particles* Europ. Phys. J. E: Soft Matter and Biological Physics, **35**, 1, 9, 2012
88. **Schouwink, P., D'Anna, V., Ley, M.B., Daku, L.M.L., Richter, B., Jensen, T.R. et al.** *Bimetallic Borohydrides in the System $M(BH_4)_2$- KBH_4 (M=Mg, Mn): On the Structural Diversity* J. Phys. Chem. C, **116**, 20, 10829-10840, 2012
89. **Serra-Crespo, P., Gobechiya, E., Ramos-Fernandez, E.V., Juan-Alcañiz, J., Martinez-Joaristi, A. et al.** *Interplay of metal node and amine functionality in NH2-MIL-53: modulating breathing behaviour through intra-framework interactions* Langmuir, **28**, 35, 12916-12922, 2012
90. **Serra-Crespo, P., Van der Veen, M.A., Gobechiya, E., Houthoofd, K., Filinchuk, Y., Kirschhock, Ch.E.A. et al.** *NH_2-MIL-53(Al): A High-Contrast Reversible Solid-State Nonlinear Optical Switch* J. Am. Chem. Soc., **134**, 20, 8314–8317, 2012
91. **Sisak, D., Baerlocher, Ch., McCusker, L.B., Gilmore, Ch.J.** *Optimizing the input parameters for powder charge flipping* J. Appl. Cryst., **45**, 1125-1135, 2012
92. **Suwarno, S., Gosselin, Y., Solberg, J.K., Maehlen, J.P., Williams, M., Krogh, B., Børresen, B.T., Rytter, E. et al.** *Selective hydrogen absorption from gaseous mixtures by BCC Ti-V alloys* Int. J. Hydrogen Energy, **37**, 5, 4127-4138, 2012
93. **Suwarno, S., Solberg, J. K., Maehlen, J.P., Krogh, B., Borresen, B. T., Ochoa--Fernandez, E. et al.** *Microstructure and hydrogen storage properties of as-cast and rapidly solidified Ti-rich Ti–V alloys* Transactions of Nonferrous Met. Soc. China, **22,** 8, 1831–1838, 2012
94. **Suwarno, S., Solberg, J.K., Maehlen, J.P., Krogh, B, Yartys, V.A.** *Influence of Cr on the hydrogen storage properties of Ti-rich Ti–V–Cr alloys* Int. J. Hydrogen Energy, **37**, 9, 7624-7628, 2012
95. **Tchougréeff, A.L., Liu, X., Müller, P., Van Beek, W., Ruschewitz, U., Dronskowski, R.** *Structural Study of CuNCN and Its Theoretical Implications: A Case of a Resonating-Valence-Bond State?* J. Phys. Chem. Lett., **3,** 22, 3360–3366, 2012
96. **Texier, Y., Deisenhofer, J., Tsurkan, V., Loidl, A., Inosov, D. S., Friemel, G., Bobroff, J.** *NMR Study in the Iron-Selenide $Rb_{0.74}Fe_{1.6}Se_2$: Determination of the Superconducting Phase as Iron Vacancy-Free $Rb_{0.3}Fe_2Se_2$* Phys. Rev. Lett., **108**, 237002-237007, 2012
97. **Tsakoumis, N.E., Voronov, A., Rønning, M., Van Beek, W., Borg, Ø., Rytter, E., Holmen, A.** *Fischer–Tropsch synthesis: An XAS/XRPD combined in situ study from catalyst activation to deactivation* J. Catalysis, **291**, 138-148, 2012
98. **Tumanov, N. A., Boldyreva, E. V.** *X-ray diffraction and Raman study of DL-alanine at high pressure: revision of phase transitions* Acta Cryst., B**68**, 412-423, 2012
99. **Valenzano, L., Vitillo, J.G., Chavan, S., Civalleri, B., Bonino, F., Bordiga, S. et al.** *Structure–activity relationships of simple molecules adsorbed on CPO-27-Ni metal–organic framework: In situ experiments vs. theory* Catalysis Today, **182**,1, 67-79, 2012
100. **Van Beek, W., Emerich, H., Urakawa, A., Palin, L., Milanesio, M., Caliandro, R., Viterbo, D., Chernyshov, D.** *Untangling diffraction intensity: modulation enhanced diffraction on ZrO_2 powder* J. Appl. Cryst., **45,** 4, 738-747, 2012

101. **Varin, R.A., Zbroniec, L., Polanski, M., Filinchuk, Y., Cerný, R.** *Mechano-chemical synthesis of manganese borohydride ($Mn(BH_4)_2$) and inverse cubic spinel (Li_2MnCl_4) in the ($nLiBH_4$ + $MnCl_2$) (n = 1, 2, 3, 5, 9 and 23) mixtures and their dehydrogenation behavior* Int. J. Hydrogen Energy, **37**, 21, 16056-16069, 2012
102. **Ve, Th., Mathisen, K., Helland, R., Karlsen, O.A., Fjellbirkeland, A., Røhr, Å.K., Andersson, K.K. et al.** *The Methylococcus capsulatus (Bath) Secreted Protein, MopE*, Binds Both Reduced and Oxidized Copper* PLoS ONE, **7**, 8, e43146, 2012
103. **Verheyen, E., Joos, L., Havenbergh, K. V., Breynaert, E., Kasian, N., Gobechiya, E. et al.** *Design of zeolite by inverse sigma transformation* Nature Materials, **11**, 1059-1064, 2012
104. **Vichery, Ch., Maurin, I., Bonville, P., Boilot, J.-P., Gacoin, Th.** *Influence of Protected Annealing on the Magnetic Properties of ?-Fe2O3 Nanoparticles* J. Phys. Chem. C, **116**, 30, 16311-16318, 2012
105. **Wang, J., Chernavskii, P. A., Khodakov, A. Y., Wang, Y**. *Structure and catalytic performance of alumina-supported copper–cobalt catalysts for carbon monoxide hydrogenation* J. Catalysis, **286**, 51-61, 2012
106. **Wragg, D.S., Akporiaye, D., Fjellvåg, H**. *Direct observation of catalyst behaviour under real working conditions with X-ray diffraction: Comparing SAPO-18 and SAPO-34 methanol to olefin catalysts* J. Catalysis, **279**, 2, 397-402, 2012
107. **Yot, P.G., Ma, Q., Haines, J., Yang, Q., Ghoufi, A., Devic, Th., Serre, Ch., Dmitriev, V. et al.** *Large breathing of the MOF MIL-47(V^{IV}) under mechanical pressure: a joint experimental–modelling exploration* Chem. Sci., **3**, 1100-1104, 2012
108. **Živkovic, I., Djokic, D. M., Herak, M., Pajic, D., Prša, K., Pattison, P. et al**. *Site-selective quantum correlations revealed by magnetic anisotropy in the tetramer system $SeCuO_3$* Phys. Rev. B **86,** 054405-054414, 2012

PhD Theses: 2011-2012

(based in part on data from SNBL)

Nikolaos E. Tsakoumis *Deactivation of cobalt based Fischer-Tropsch synthesis catalysts.* Norwegian University of Science and Technology (Trondheim), 2011

Belay Zeleke Dilnesa *Fe-containing hydrates and their fate during cement hydration: thermodynamic data and experimental study*. École Polytechnique Fédérale de Lausanne (2011)